Hrs plays crucial roles in HCV and exosomal secretion

Since Hrs is to be required for exosome secretion (Tamai et al., 2010), we examined the roles of membrane traffic-related proteins in HCV secretion. For this study, we established an Hrs-depleted Huh7 cell line using shRNA against human Hrs (Fig. 2A), and Huh7 cell lines that overexpressed wild-type VPS4B, and an ATPase-negative VPS4B (VPS4B^{E228Q}, Fig. 2B). We also prepared knock-down Huh7 cell lines for AMSH, a deubiquitination enzyme that binds the ESCRT-III complex, and for Rab27a, a Rab GTPase required for exosome secretion, using specific shRNAs (Figs. 2C and D).

First, we confirmed that Hrs plays a crucial role in exosome secretion in Huh7 cells. Exosome secretion of the control Huh7 cells was clearly increased by 48 h of stimulation with Ca^{2+} ionophore A23187, a well-established stimulator for exosome secretion (Savina et al., 2005), whereas a smaller increase was observed in the Hrs-depleted Huh7 cells (Fig. 3). These data confirmed Hrs's crucial role in the exosome secretion of Huh7 cells.

Next, using the various Huh7 cell lines, we analyzed whether membrane-traffic-related proteins are involved in HCV release. We first compared the amount of HCV-RNA in the culture supernatants of the Huh7 cell lines. The amount of HCV-RNA was significantly lower in the supernatant of the Hrs-depleted cells from days 3 to 5 post-infection (Fig. 4A). Similarly, overexpression of the dominant-negative VPS4B decreased the HCV-RNA production in Huh7 cells (Fig. 4B), consistent with a previous report (Corless et al., 2010). In contrast, there was no difference in the HCV release between the AMSH-depleted and control Huh7 cells (Fig. 4C). However, HCV-RNA was dramatically decreased in the Rab27a-depleted Huh7 cells (Fig. 4D).

We also confirmed the amount of HCV by measuring the HCV infectious titer in the supernatant. The virus titer was significantly decreased in the absence of Hrs, Rab27a and overexpressed ATPase defective-VPS4B, but not in the absence of AMSH (Fig. 4E). These data were compatible with the amount of HCV-RNA.

Since Hrs-depletion decreased the Huh7 cells' growth rate (data not shown), we also examined the amount of HCV using X-ray-irradiated cells to inhibit the cell proliferation, and eliminate the cell growth effect. In a preliminary experiment, we confirmed that irradiation with X-rays (25 Gy) was enough to inhibit the Huh7 cell proliferation completely (data not shown). The amount of HCV-RNA in the supernatant was decreased in the Hrs-depleted irradiated Huh7 cells compared with control cells (Fig. 5). These data together indicated that Hrs plays a crucial role in HCV secretion.

Analysis of intracellular HCV-RNA

We next assessed whether the decreased HCV release observed in the Huh7 cell lines reflected a decrease in viral reproduction, by
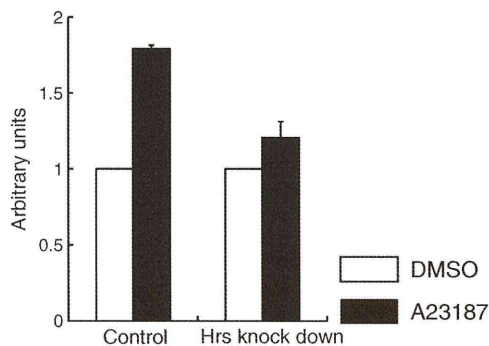
examining the intracellular HCV-RNA. In the Hrs-depleted Huh7 cells, no significant decrease in the amount of intracellular HCV-RNA was found (Fig. 6A). Similar results were obtained in the Huh7 cells expressing dominant-negative VPS4B and those with AMSH-depletion (Figs. 6B and C). In the Rab27a-depleted Huh7 cells, the amount of intracellular HCV-RNA was decreased on day 5. (Fig. 6D).

Next, we quantified the amount of intracellular HCV core protein using Western blot analysis. The expression of core protein was almost the same between in the Hrs-depleted Huh7 cells and the control cells on days 5 and 7 post-infection (Fig. 6E). These results suggested that Hrs is not involved in HCV replication or translation.
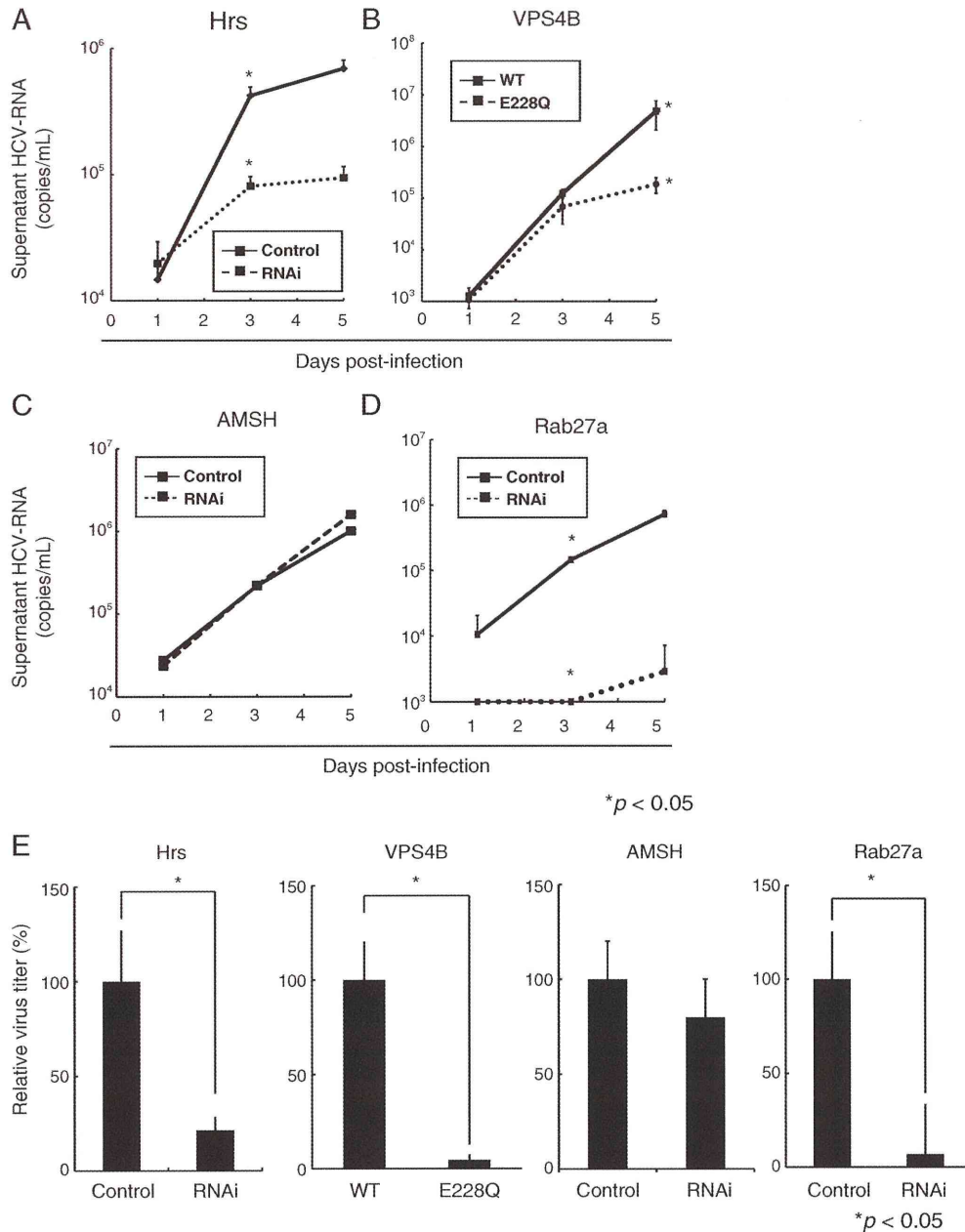
Since the HCV-RNA in the supernatant was decreased in Hrs-depleted Huh7 cells without any decrease in the intracellular HCV-RNA or core protein, the assembly and/or release of HCV might be impaired in the absence of Hrs. Hence, we examined the effect of Hrs depletion on the amount of intracellular infectious HCV particles by performing a focus-forming unit assay. Intracellular infectious HCV particles were decreased in Huh7 cells with Hrs-depletion and Rab27a-depletion and those expressing dominant-negative VPS4B compared with control cells on day 5 post-infection (Figs. 6F to I). These data suggested that Hrs is required at least for HCV assembly.

Discussion

This study addressed the relationship between the ESCRT machinery and HCV viral release. Although the initial studies on ESCRT proteins mostly focused on their role in the endosomal sorting and lysosomal digestion of membrane-bound receptors, there is accumulating evidence that they also play important roles in MVB formation (Wollert and Hurley, 2010). ESCRT executes scission of the endosomal limiting membranes to form the intraluminal vesicles that characterize MVBs and of the plasma membrane to release intraluminal microvesicles into the extracellular environment as exosomes (de Gassart et al., 2004). Here we demonstrated that an ESCRT-0 component, Hrs, is crucial for HCV release through the exosome secretion pathway.

Previous reports suggested that Hrs recruits ESCRT-I complex components, including Tsg101, VPS28, and VPS37, and initiates the ESCRT pathway. The ESCRT-I component Tsg101 was also reported to form a complex with HIV-1 Gag, which promotes an Hrs-independent ESCRT mechanism for HIV release (Pornillos et al., 2003). Similarly, Tsg101 is involved in the release of human T-cell leukemia virus (HTLV)-I, because Tsg101 depletion inhibits HTLV-I budding (Blot et al., 2004). These viruses utilize not only ESCRT-I but also its downstream machinery, including ESCRT-III and VPS4. This is also the case for HCV, because ESCRT proteins such as ESCRT-III, VPS4, TSG101, and Alix contribute to HCV release (Ariumi et al., 2011; Corless et al., 2010). In this context, VPS4 is one of the last and most potent molecules in the ESCRT pathway, and the dependence of enveloped-virus budding on the ESCRT machinery has been proved in several cases by showing that the budding is VPS4-dependent. Taking all these data together, we concluded that HCV takes advantage of the entire ESCRT machinery for its release.

In this study, Hrs depletion attenuated both HCV release into the supernatant and the amount of infectious particles in the cytoplasm, but not the amount of HCV-RNA in the cytoplasm, suggesting that Hrs is involved in HCV assembly. A previous study suggested that the formation of HCV virions is closely connected to lipid droplets and the endoplasmic reticulum (ER) (Miyanari et al., 2007). Here we observed two HCV antigens, the core protein and E2, within MVBs in Huh7 cells, indicating that HCV probably takes advantage of the MVBs themselves for its assembly. In this study, AMSH, which does not affect MVB formation (data not shown), was not required for HCV release, supporting our hypothesis. The relationship between the ER and MVBs is not fully understood, but a recent study suggested that direct membrane contact occurs between them (Eden et al.,

Fig. 3. Hrs affects exosome release in Huh7 cells. Measurement of exosomes under stimulation with a Ca^{2+} ionophore (A23187), using a protein assay. Control and Hrs-knock-down Huh7 cells were incubated with 1 μM A23187 for 48 h.

Fig. 4. Hrs, VPS4B, and Rab27a, but not AMSH, affect HCV release. (A to D) HCV-RNA in the culture supernatant on the indicated day after infection, measured using real-time PCR. Huh7 cells were infected with HCV (MOI = 0.01). (E) Infectious HCV particles in the supernatant were measured by a focus-forming unit assay at day 5 post-infection.

2010). Although the detailed mechanisms are not fully elucidated, we propose that normal trafficking via MVBs is required for the formation of complete HCV particles.

In this study we found the relationship between HCV and exosome from three experiments. First, by using immunoelectron microscopy, we demonstrated that HCV core protein and CD63 colocalized each other in MVB. Second, the confocal microscopy analyses revealed that exosomal marker N-Rh-PE colocalized with the core protein. Third, purified exosomal fraction possessed infectivity to Huh7 cells. These results suggest that HCV particles indeed colocalize with exosomes, and contain exosome marker proteins. This notion is not surprising because various viruses have been shown to acquire parts of host cell-derived proteins (Kolegraff et al., 2006). These phenomenons seem to reflect a fact that a number of

virus carry host factors either during the assembly, or the release from their respective host cells. In Fig. 1A, the peaks for the HCV core protein and CD63 do not entirely correspond (1.18 g/ml and 1.15 g/ml, respectively). In general, HCV particles and exosomes in diameter are very similar (50 nm and 30–100 nm, respectively). On the other hand, HCV particles contain genomes which consist of a positive-sense RNA molecule approximately 9.6 kb in length. It is possible that the density of HCV particles is somewhat higher than that of exosomes. Further study will be required to elucidate how HCV particles and exosomes were similarly or differentially produced in MVB.

The detailed mechanisms by which HCV utilizes the ESCRT machinery for its release are still unknown. Capsid proteins of several viruses, such as HIV and HTLV-1 interact with ESCRT proteins via the
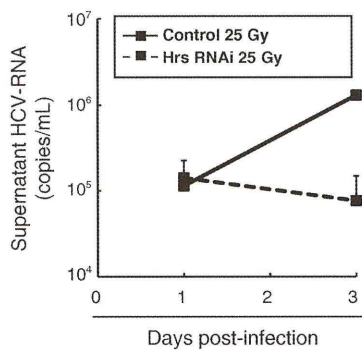
Fig. 5. Hrs affects HCV release in irradiated Huh7 cells. Control or Hrs knock-down Huh7 cells were irradiated with X-rays (25 Gy) and infected with HCV (MOI = 0.1). The results are the mean and SD from three parallel samples.

capsid-proteins' L-domains. This interaction recruits ESCRT to the site of capsid accumulation, and contributes to the budding of capsid-captured membranes, scission, and the release of virions, using similar mechanisms to those involved in MVB formation (McDonald and Martin-Serrano, 2009). Therefore, it is tempting to speculate a similar viral structure-ESCRT interaction scenario for HCV release. However, we found no canonical L-domains such as PT/SAP, YPXL, PPXY, or LYPXnL, within the amino acid sequence of HCV proteins. In the case of HIV-1, a previous report suggested that the HIV-1 Gag proteins are ubiquitinated and that this ubiquitination is required for HIV-1 release (Gottwein and Krausslich, 2005). Concordantly, the HCV core protein is reported to be ubiquitinated by E6AP (Shirakura et al., 2007). Thus, the ESCRTs might interact with viral proteins through the ESCRT proteins' ubiquitin-binding domain. Because Hrs possesses two ubiquitin-binding regions, UIM and VHS, Hrs may recognize the ubiquitinated HCV core proteins and sort them to the viral budding site in the MVBs, thereby enabling virion release.
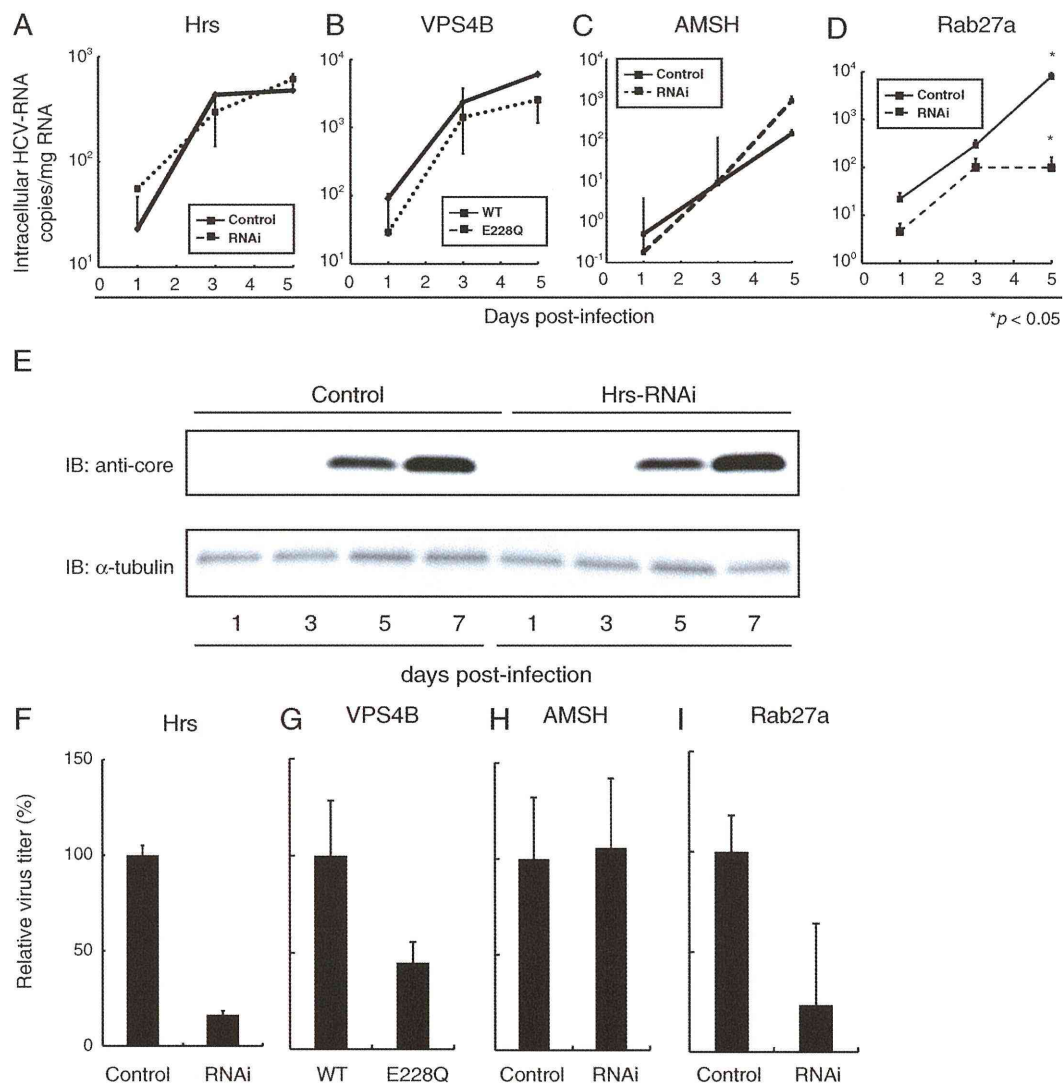
Fig. 6. No alteration in HCV-RNA replication in Hrs-depleted cells. (A to D) Intracellular HCV-RNA was measured in various Huh7 cell lines on the indicated day after infection. Values were normalized to the total RNA. The results are the mean and SD from three parallel samples. In VPS4B-expressing Huh7 cells, the difference is not significant through days 1 to 5. (E) Western blot analysis of HCV core protein. Total lysates were prepared from control and Hrs-depleted Huh7 cells on the indicated day post-infection and analyzed by immunoblotting with an anti-core antibody. Data are representative of three independent experiments. (F to I) Intracellular infectious HCV particles were measured by a focus-forming unit assay at day 5 post-infection.

A previous study suggested that human herpes virus-6 (HHV-6) is released together with internal vesicles through MVBs by the cellular exosomal pathway: HHV-6 undergoes maturation in the trans-Golgi network (TGN) and post-TGN-derived vacuoles, which express an exosomal marker, CD63, and MVBs contain HHV-6 envelope glycoproteins along with CD63 (Mori et al., 2008). In addition, HIV virions released into the culture supernatant also contain CD63 (Gould et al., 2003), and CD63-positive exosomes derived from HIV-infected cells contain HIV Gag proteins (Booth et al., 2006). Here we showed that CD63-positive exosomal fractions can also contain HCV particles. Taken together, these observations support the idea that exosomal secretion and the budding of HCV, HHV6, and HIV share overlapping pathways.

Conclusion

Since we here provide evidence that Hrs is important in exosome secretion and HCV release, Hrs may be one of the key players in HCV release, through the exosomal pathway. Controlling this pathway could become one of novel therapeutic strategies for chronic viral infections.

Materials and methods

Ethics statements

This study was conducted according to the principles expressed in the Declaration of Helsinki. The study was approved by the research committees of the Miyagi Cancer Center and Tohoku University.

Cells

Huh7 and Huh7.5.1 (gift from Dr. Chisari, The Scripps Research Institute, CA) cells were maintained in Dulbecco's modified essential medium containing 10% fetal calf serum and antibiotics. To express Hrs-specific short hairpin RNA (shRNA), a retroviral vector was generated as described previously (Tamai et al., 2007). In brief, a sequence encoding human Hrs-specific shRNA, was inserted into pSIREN-RetroQ (BD Biosciences) to make pSIREN-RetroQ-Hrs. The target sequence consisted of nucleotides 302–320 (5′-AGG-TAAACGTCCGTAACAA-3′) of the human hrs cDNA. A control plasmid, pSIREN-RetroQ-Luc, targeted bp 413–434 of firefly luciferase (5′-GCAATAGTTCACGCTGAAAAG-3′). The retrovirus was prepared as previously described (Tamai et al., 2007). A human AMSH-specific short hairpin RNA (shRNA), pSIREN-RetroQ-AMSH, was also generated using pSIREN-RetroQ (Kyuuma et al., 2007). The target sequence within the human AMSH cDNA was nucleotides 651–669 (5′-GCAG-CAATTGGAACAGGAA-3′). A human Rab27a-specific shRNA lentiviral vector was purchased from Sigma. LDH assay was performed according to the manufacturer's protocol (Roche, Basel, Switzerland).

Isolation and purification of exosomes

Exosomes were purified as previously described (Ostrowski et al., 2010). In brief, the cell culture medium was centrifuged for 10 min at $300 \times g$, 10 min at $1200 \times g$, and 30 min at $10,000 \times g$ to remove cells and debris. The supernatant obtained from the last spin was then centrifuged for 60 min at $100,000 \times g$, and the pellet was solubilized in lysis buffer (1% Nonidet P-40, 20 mM Tris–HCl (pH 7.5), 150 mM NaCl, 1 mM EDTA, 1 mM phenylmethylsulfonyl fluoride, and 20 µg/ml aprotinin) and analyzed by BCA protein assay (Pierce, Rockford, IL, USA), according to the manufacturer's protocol. For sucrose density gradient centrifugation, sucrose gradients were prepared according to a former procedure (Abe and Davies, 1986). In brief, 5 ml 72% sucrose/PBS was overlaid with 5 ml 8.4% sucrose/PBS in 10 ml tubes, and the tubes stoppered and kept horizontal for 3 h at

room temperature, after which they were slowly returned to the upright position. The exosomal suspension was layered onto a gradient sucrose and centrifuged at $100,000 \times g$ for 20 h in a Beckmann SW41Ti rotor.

Western blotting

Immunoblotting was performed as described previously (Takeuchi et al., 1999). In brief, total cell lysates were prepared with NP-40-containing lysis buffer (described above). The lysates were pre-cleared by centrifugation ($10,000 \times g$) for 20 min at 4 °C, and the supernatants were separated by SDS-PAGE and transferred onto polyvinyl difluoride (PVDF) membranes (Millipore). After being blocked with 5% nonfat milk in Tris-buffered saline (TBS) containing 0.1% Tween 20, the membranes were probed with the indicated primary antibodies. After another wash, the membranes were probed with HRP-conjugated secondary antibodies (Cell Signaling). For dot-blot analyses, cell lysates were spotted onto PVDF membranes. The membranes were blocked as described above and incubated with the indicated antibodies.

Generation and quantification of cell culture HCV RNA and infectious titer

The HCV strain JFH-1 was a gift from Dr. T. Wakita (National Institute of Infectious Diseases, Japan) (Wakita et al., 2005). Cell-culture-derived, infectious HCV was generated as described previously (Wakita et al., 2005). The HCV was quantified as follows: RNA was extracted from the Huh7 culture supernatant using the QIAamp Viral RNA Kit (Qiagen, Valencia, CA). The HCV RNA was quantified by real-time reverse transcription polymerase chain reaction using TaqMan EZ RT-PCR Core Reagents (Applied Biosystems, Foster City, CA), according to the manufacturer's protocol, using the published primers and probe (Takeuchi et al., 1999). The filtered (0.45 µm) culture supernatant of HCV-infected Huh-7.5.1 cells containing 2×10^8 HCV RNA copies/ml (equivalent to 9.7×10^4 focus-forming units [ffu]/ml) was used for experiments. To analyze HCV-RNA in the supernatant, Huh7 cells (2×10^5 cells in 6-well plate) were infected with JFH-1 (multiplicity of infection, MOI = 0.01), washed with PBS twice after 4 h, the supernatants were collected, and the cells were reseeded at 2×10^5 cells per 6-well plate at the indicated times. Huh7 cells were irradiated with X-rays (25 Gy) before infection to exclude the effect of cell proliferation in some experiments. To quantify the intracellular HCV titer, infected Huh7 cells were harvested at the indicated times and lysed by three freeze-thaw cycles. The virus titer was determined by focus-forming unit assay, as previously described (Kato et al., 2006).

Antibodies for immunoelectron microscopy

An anti-HCV-core mouse monoclonal antibody (mAb) (2H9, a gift from Dr. Wakita, National Institute of Infectious Diseases, Japan) and a human anti-E2 mAb (CBH5, a gift from Dr. Foung, Department of Pathology, Stanford School of Medicine) were used as primary antibodies. As secondary antibodies for immunoelectron microscopy, 5-nm-colloidal-immunogold-labeled anti-mouse goat IgG and 5-nm-immunogold-labeled anti-human goat IgG antibodies (EY Laboratories, San Mateo, CA) were used.

Quantitative real-time polymerase chain reaction

To confirm the knock-down of Rab27a, quantitative real-time PCR was performed. Total RNA was prepared from cells with the RNeasy Mini kit (Qiagen). Complementary deoxyribonucleic acid (cDNA) was synthesized using an oligo d(T)12–18 primer with a Primescript reverse transcriptase (Takara Bio Inc, Japan) and subjected to quantitative real-

time PCR using a LightCycler 480 and the SYBR Green I Master kit (Roche Diagnostics). The primer sequences were, for GAPDH, 5′-CTCTGCTCCTCCTGTTCGAC-3′ and 5′-GACAAGCTTCCCGTTCTCAG-3′; and for Rab27a, 5′-TGGAGGACCAGAGAGTAGTGAAA-3′ and 5′-AGTTT-CAAAGTAGGGGATTCCA-3′.

Phenotypic analysis of cells by flow cytometry

Cells were assessed for VPS4B-GFP expression by fluorescent multicolor flow cytometry (FACSCantoII, Becton Dickinson, San Jose, CA) as previously described (Tamai et al., 2010).

Immunoelectron microscopy

To analyze the localization of the HCV antigen in MVBs, Huh7 cells infected with JFH-1 were fixed with 1% glutaraldehyde in phosphate-buffered saline (PBS, pH 7.2) at 4 °C for 2 h. The fixed cells were washed six times with PBS and dehydrated in a graded ethanol series. The samples were then embedded in Lowicryl K4M resin (Polyscience, Warrington, PA, USA), and allowed to polymerize in a UV irradiator (DOSAKA EM, Kyoto, Japan) at − 20 °C for 2 days and then at room temperature for 2 days. Ultrathin sections were cut using an ultramicrotome (Sorvall MT-5000, Du Pont, CT, USA) and mounted on a nickel grid (300 mesh) supported by a carbon-coated collodion film. The ultrathin sections on the grid were treated with 5% normal goat serum in PBS to block non-specific reactions. The sections were then reacted with drops of primary antibody at 4 °C for 8 h, washed with PBS, reacted with secondary antibody for 1 h at room temperature, and washed again with PBS. The immunostained sections were fixed in 1% glutaraldehyde in PBS for 15 min and washed three times with distilled water. Finally, the sections were subjected to contrast-enhanced staining with 0.01% ruthenium red (Wako Pure Chemicals, Osaka, Japan) and 0.5% osmium tetroxide in PBS at room temperature for 10 min, further with 4%(w/v) uranyl acetate in distilled water for 15 min at room temperature, and observed under a transmission electron microscope (H-7650, Hitachi, Tokyo, Japan).

For double-staining of immunoelectron microscopy, post-embedding gold was carried out as described previously (Iwata et al., 1995). Mouse anti-HCV-core IgG (2H9, diluted 50×) and rabbit anti-CD63 IgG (sc-15363 Santa Cruz, diluted ×5) were used.

Acknowledgments

References

Abe, S., Davies, E., 1986. Quantitative Analysis of Polysome Profiles Using a Baseline from Uncentrifuged Blank Gradients, 31. Memories of the College of Agriculture, Ehime University, pp. 187–199.

Ariumi, Y., Kuroki, M., Maki, M., Ikeda, M., Dansako, H., Wakita, T., Kato, N., 2011. The ESCRT system is required for hepatitis C virus production. PLoS One 6, e14517.

Asao, H., Sasaki, Y., Arita, T., Tanaka, N., Endo, K., Kasai, H., Takeshita, T., Endo, Y., Fujita, T., Sugamura, K., 1997. Hrs is associated with STAM, a signal-transducing adaptor molecule. Its suppressive effect on cytokine-induced cell growth. J. Biol. Chem. 272, 32785–32791.

Asselah, T., Benhamou, Y., Marcellin, P., 2009. Protease and polymerase inhibitors for the treatment of hepatitis C. Liver Int. 29 (Suppl. 1), 57–67.

Blot, V., Perugi, F., Gay, B., Prevost, M.C., Briant, L., Tangy, F., Abriel, H., Staub, O., Dokhelar, M.C., Pique, C., 2004. Nedd4.1-mediated ubiquitination and subsequent recruitment of Tsg101 ensure HTLV-1 Gag trafficking towards the multivesicular body pathway prior to virus budding. J. Cell Sci. 117, 2357–2367.

Booth, A.M., Fang, Y., Fallon, J.K., Yang, J.M., Hildreth, J.E., Gould, S.J., 2006. Exosomes and HIV Gag bud from endosome-like domains of the T cell plasma membrane. J. Cell Biol. 172, 923–935.

Burlone, M.E., Budkowska, A., 2009. Hepatitis C virus cell entry: role of lipoproteins and cellular receptors. J. Gen. Virol. 90, 1055–1070.

Chen, B.J., Lamb, R.A., 2008. Mechanisms for enveloped virus budding: can some viruses do without an ESCRT? Virology 372, 221–232.

Corless, L., Crump, C.M., Griffin, S.D., Harris, M., 2010. Vps4 and the ESCRT-III complex are required for the release of infectious hepatitis C virus particles. J. Gen. Virol. 91, 362–372.

de Gassart, A., Geminard, C., Hoekstra, D., Vidal, M., 2004. Exosome secretion: the art of reutilizing nonrecycled proteins? Traffic 5, 896–903.

Denzer, K., Kleijmeer, M.J., Heijnen, H.F., Stoorvogel, W., Geuze, H.J., 2000. Exosome: from internal vesicle of the multivesicular body to intercellular signaling device. J. Cell Sci. 113 (Pt 19), 3365–3374.

Eden, E.R., White, I.J., Tsapara, A., Futter, C.E., 2010. Membrane contacts between endosomes and ER provide sites for PTP1B-epidermal growth factor receptor interaction. Nat. Cell Biol. 12, 267–272.

Evans, M.J., von Hahn, T., Tscherne, D.M., Syder, A.J., Panis, M., Wolk, B., Hatziioannou, T., McKeating, J.A., Bieniasz, P.D., Rice, C.M., 2007. Claudin-1 is a hepatitis C virus co-receptor required for a late step in entry. Nature 446, 801–805.

Gottwein, E., Krausslich, H.G., 2005. Analysis of human immunodeficiency virus type 1 Gag ubiquitination. J. Virol. 79, 9134–9144.

Gould, S.J., Booth, A.M., Hildreth, J.E., 2003. The Trojan exosome hypothesis. Proc. Natl. Acad. Sci. U.S.A. 100, 10592–10597.

Iwata, K., Yamamoto, A., Satoh, S., Ohyama, Y., Tashiro, Y., Setoguchi, T., 1995. Quantitative immunoelectron microscopic analysis of the localization and induction of 25-hydroxyvitamin D3 24-hydroxylase in rat kidney. J. Histochem. Cytochem. 43, 255–262.

Kato, T., Date, T., Murayama, A., Morikawa, K., Akazawa, D., Wakita, T., 2006. Cell culture and infection system for hepatitis C virus. Nat. Protoc. 1, 2334–2339.

Kolegraff, K., Bostik, P., Ansari, A.A., 2006. Characterization and role of lentivirus-associated host proteins. Exp. Biol. Med. (Maywood) 231, 252–263.

Komada, M., Kitamura, N., 1995. Growth factor-induced tyrosine phosphorylation of Hrs, a novel 115-kilodalton protein with a structurally conserved putative zinc finger domain. Mol. Cell. Biol. 15, 6213–6221.

Kyuuma, M., Kikuchi, K., Kojima, K., Sugawara, Y., Sato, M., Mano, N., Goto, J., Takeshita, T., Yamamoto, A., Sugamura, K., Tanaka, N., 2007. AMSH, an ESCRT-III associated enzyme, deubiquitinates cargo on MVB/late endosomes. Cell Struct. Funct. 31, 159–172.

Lai, C.K., Jeng, K.S., Machida, K., Lai, M.M., 2010. Hepatitis C virus egress and release depend on endosomal trafficking of core protein. J. Virol. 84, 11590–11598.

Lenassi, M., Cagney, G., Liao, M., Vaupotic, T., Bartholomeeusen, K., Cheng, Y., Krogan, N.J., Plemenitas, A., Peterlin, B.M., 2010. HIV Nef is secreted in exosomes and triggers apoptosis in bystander CD4 + T cells. Traffic 11, 110–122.

Masciopinto, F., Giovani, C., Campagnoli, S., Galli-Stampino, L., Colombatto, P., Brunetto, M., Yen, T.S., Houghton, M., Pileri, P., Abrignani, S., 2004. Association of hepatitis C virus envelope proteins with exosomes. Eur. J. Immunol. 34, 2834–2842.

McDonald, B., Martin-Serrano, J., 2009. No strings attached: the ESCRT machinery in viral budding and cytokinesis. J. Cell Sci. 122, 2167–2177.

Miyanari, Y., Atsuzawa, K., Usuda, N., Watashi, K., Hishiki, T., Zayas, M., Bartenschlager, R., Wakita, T., Hijikata, M., Shimotohno, K., 2007. The lipid droplet is an important organelle for hepatitis C virus production. Nat. Cell Biol. 9, 1089–1097.

Mori, Y., Koike, M., Moriishi, E., Kawabata, A., Tang, H., Oyaizu, H., Uchiyama, Y., Yamanishi, K., 2008. Human herpesvirus-6 induces MVB formation, and virus egress occurs by an exosomal release pathway. Traffic 9, 1728–1742.

Murray, C.L., Jones, C.T., Rice, C.M., 2008. Architects of assembly: roles of Flaviviridae non-structural proteins in virion morphogenesis. Nat. Rev. Microbiol. 6, 699–708.

Ostrowski, M., Carmo, N.B., Krumeich, S., Fanget, I., Raposo, G., Savina, A., Moita, C.F., Schauer, K., Hume, A.N., Freitas, R.P., Goud, B., Benaroch, P., Hacohen, N., Fukuda, M., Desnos, C., Seabra, M.C., Darchen, F., Amigorena, S., Moita, L.F., Thery, C., 2010. Rab27a and Rab27b control different steps of the exosome secretion pathway. Nat. Cell Biol. 12, 19–30 (sup pp 11–13).

Pan, B.T., Teng, K., Wu, C., Adam, M., Johnstone, R.M., 1985. Electron microscopic evidence for externalization of the transferrin receptor in vesicular form in sheep reticulocytes. J. Cell Biol. 101, 942–948.

Pornillos, O., Higginson, D.S., Stray, K.M., Fisher, R.D., Garrus, J.E., Payne, M., He, G.P., Wang, H.E., Morham, S.G., Sundquist, W.I., 2003. HIV Gag mimics the Tsg101-recruiting activity of the human Hrs protein. J. Cell Biol. 162, 425–434.

Savina, A., Fader, C.M., Damiani, M.T., Colombo, M.I., 2005. Rab11 promotes docking and fusion of multivesicular bodies in a calcium-dependent manner. Traffic 6, 131–143.

Shiina, M., Rehermann, B., 2008. Cell culture-produced hepatitis C virus impairs plasmacytoid dendritic cell function. Hepatology 47, 385–395.

Shirakura, M., Murakami, K., Ichimura, T., Suzuki, R., Shimoji, T., Fukuda, K., Abe, K., Sato, S., Fukasawa, M., Yamakawa, Y., Nishijima, M., Moriishi, K., Matsuura, Y., Wakita, T., Suzuki, T., Howley, P.M., Miyamura, T., Shoji, I., 2007. E6AP ubiquitin ligase mediates ubiquitylation and degradation of hepatitis C virus core protein. J. Virol. 81, 1174–1185.

Takeuchi, T., Katsume, A., Tanaka, T., Abe, A., Inoue, K., Tsukiyama-Kohara, K., Kawaguchi, R., Tanaka, S., Kohara, M., 1999. Real-time detection system for quantification of hepatitis C virus genome. Gastroenterology 116, 636–642.

Tamai, K., Tanaka, N., Nara, A., Yamamoto, A., Nakagawa, I., Yoshimori, T., Ueno, Y., Shimosegawa, T., Sugamura, K., 2007. Role of Hrs in maturation of autophagosomes in mammalian cells. Biochem. Biophys. Res. Commun. 360, 721–727.

Tamai, K., Tanaka, N., Nakano, T., Kakazu, E., Kondo, Y., Inoue, J., Shiina, M., Fukushima, K., Hoshino, T., Sano, K., Ueno, Y., Shimosegawa, T., Sugamura, K., 2010. Exosome

secretion of dendritic cells is regulated by Hrs, an ESCRT-0 protein. Biochem. Biophys. Res. Commun. 399, 384–390.

Tanaka, Y., Tanaka, N., Saeki, Y., Tanaka, K., Murakami, M., Hirano, T., Ishii, N., Sugamura, K., 2008. c-Cbl-dependent monoubiquitination and lysosomal degradation of gp130. Mol. Cell. Biol. 28, 4805–4818.

Tanida, I., Fukasawa, M., Ueno, T., Kominami, E., Wakita, T., Hanada, K., 2009. Knockdown of autophagy-related gene decreases the production of infectious hepatitis C virus particles. Autophagy 5, 937–945.

van Niel, G., Porto-Carreiro, I., Simoes, S., Raposo, G., 2006. Exosomes: a common pathway for a specialized function. J. Biochem. 140, 13–21.

Wakita, T., Pietschmann, T., Kato, T., Date, T., Miyamoto, M., Zhao, Z., Murthy, K., Habermann, A., Krausslich, H.G., Mizokami, M., Bartenschlager, R., Liang, T.J., 2005. Production of infectious hepatitis C virus in tissue culture from a cloned viral genome. Nat. Med. 11, 791–796.

Wollert, T., Hurley, J.H., 2010. Molecular mechanism of multivesicular body biogenesis by ESCRT complexes. Nature 464, 864–869.

Hrs Recognizes a Hydrophobic Amino Acid Cluster in Cytokine Receptors during Ubiquitin-independent Endosomal Sorting*[S]

Yuji Amano[‡], Yuki Yamashita[‡], Katsuhiko Kojima[‡], Kazuhisa Yoshino[‡], Nobuyuki Tanaka[§], Kazuo Sugamura[¶], and Toshikazu Takeshita[‡1]

From the [‡]Department of Microbiology and Immunology, Shinshu University School of Medicine, 3-1-1 Asahi, Matsumoto, Nagano 390-8621, Japan and the [§]Division of Immunology and [¶]Miyagi Cancer Center Research Institute, 47-1 Nodayama, Medeshima-Shiode, Natori 981-1293, Japan

Hepatocyte growth factor-regulated tyrosine kinase substrate (Hrs) is a component of the ESCRT-0 protein complex that captures ubiquitylated cargo proteins and sorts them to the lysosomal pathway. Although Hrs acts as a key transporter for ubiquitin-dependent endosomal sorting, we previously reported that Hrs is also involved in ubiquitin-independent endosomal sorting of interleukin-2 receptor β (IL-2Rβ). Here, we show direct interactions between bacterially expressed Hrs and interleukin-4 receptor α (IL-4Rα), indicating that their binding is not required for ubiquitylation of the receptors, similar to the case for IL-2Rβ. Examinations of the Hrs binding regions of the receptors reveal that a hydrophobic amino acid cluster in both IL-2Rβ and IL-4Rα is essential for the binding. Whereas the wild-type receptors are delivered to LAMP1-positive late endosomes, mutant receptors lacking the hydrophobic amino acid cluster are sorted to lysobisphosphatidic acid-positive late endosomes rather than LAMP1-positive late endosomes. We also show that the degradation of these mutant receptors is attenuated. Accordingly, Hrs functions during ubiquitin-independent endosomal sorting of the receptors by recognizing the hydrophobic amino acid cluster. These findings suggest the existence of a group of cargo proteins that have this hydrophobic amino acid cluster as a ubiquitin-independent sorting signal.

Endosomal sorting of cell surface receptors plays a key role in the destiny of the receptors, as some receptors in sorting endosomes are recycled back to the plasma membrane, whereas others are delivered to the lysosome for degradation and attenuation of receptor-mediated signal transduction. During endosomal sorting, ubiquitylation of the receptors serves as a sorting signal (1–3). Internalized receptors are pinched off from the plasma membrane into vesicles and then caught by the endosomal sorting complex required for transport (ESCRT)[2] protein

complexes ESCRT-I and ESCRT-II at the late endosome stage. These ESCRT complexes, which consist of class E vacuolar protein sorting (Vps) proteins, recognize ubiquitylated cargo or receptor proteins via subunits that interact directly with the ubiquitylated proteins (4–6). An ESCRT-I complex recruits an ESCRT-II complex on the endosomal membrane, and the recruited ESCRT-II complex stimulates the assembly of an ESCRT-III complex, which acts as the membrane abscission machinery for the budding membrane to form a multivesicular body (MVB) (7–11). Mature MVBs fuse with the lysosome, thereby releasing the receptor-containing vesicles into the hydrolytic lumen for degradation.

Hepatocyte growth factor-regulated tyrosine kinase substrate (Hrs) and signal transducing adaptor molecule (STAM) were identified as phosphotyrosine proteins after stimulation with hepatocyte growth factor (12) and interleukin-2 (IL-2) (13), respectively. Hrs (Vps27 in yeast) is associated with STAM (Hse1 in yeast) (14), and both proteins contain a ubiquitin-interacting motif (UIM) domain that binds to ubiquitylated cargo proteins (15–18). Because Hrs and STAM complexes recruit ESCRT-I during the process for endosomal sorting of ubiquitylated cargo or receptor proteins, these complexes are sometimes referred to as ESCRT-0 (19). Mutations of the UIM domain of Hrs abrogate its ability to bind to ubiquitylated proteins (20) and consequently prevent ubiquitylated cargo proteins from being sorted into the vacuolar lumen (21). Accordingly, Hrs appears to function as a critical transporter in the early stage of ubiquitin-dependent endosomal sorting.

IL-2 is a cytokine that is mainly produced by T cells and promotes T cell growth, differentiation, and activation of various types of hematopoietic cells through its interactions with IL-2 receptor (IL-2R) complexes. Functional IL-2R complexes are composed of α, β, and γc chains or β and γc chains, indicating that the β and γc chains are indispensable for the formation of functional IL-2R complexes (22). We previously found a direct interaction between bacterially expressed IL-2Rβ and Hrs, indicating that this binding is independent of ubiquitin (23). Furthermore, an IL-2Rβ mutant lacking the Hrs binding region exhibited impaired endosomal sorting to LAMP1-posi-

---

[S] The on-line version of this article (available at http://www.jbc.org) contains supplemental Figs. S1–S6.

[1] To whom correspondence should be addressed. Tel.: 81-263-37-2614; Fax: 81-263-37-2616; E-mail: takesit@shinshu-u.ac.jp.

[2] The abbreviations used are: ESCRT, endosomal sorting complex required for transport; GGA, Golgi-localized, γ-ear-containing, Arf-binding protein; IL-2Rβ, IL-2 receptor β chain; IL-4Rα, IL-4 receptor α chain; Hrs, hepatocyte growth factor-regulated tyrosine kinase substrate; STAM, signal transduc-

ing adaptor molecule; MVB, multivesicular body; UIM, ubiquitin interacting motif; Vps, vacuolar protein sorting; DTSSP, dithiobis(sulfosuccinimidyl-propionate); LBPA, lysobisphosphatidic acid; MEF, mouse embryonic fibroblast.

tive late endosomes, and the degradation rate of the IL-2Rβ mutant was diminished compared with that of wild-type IL-2Rβ (23). These findings led us to propose the following two hypotheses; 1) there is a group of cytokine receptors that interact with Hrs in a ubiquitin-independent manner, because it does not follow that only IL-2Rβ interacts with Hrs in this manner, and 2) there is a motif that interacts with Hrs in the cytoplasmic region of such receptors. In the present study, we tried to identify a ubiquitin-independent Hrs binding motif present in cytokine receptors.

EXPERIMENTAL PROCEDURES

Plasmids—Expression vectors containing HA-tagged wild-type Hrs (pKU-HrsHA) and its derivative mutants HrsHAd257–277 (dUIM) and HrsHAd428–466 were used (23). pME18s-IL-4Rα, which contains a human IL-4Rα cDNA, was kindly provided by S. Watanabe (The University of Tokyo, Tokyo, Japan). An expression vector for FLAG-tagged IL-4Rα (FLAG-IL4Rα) was generated by inserting the FLAG epitope (DYKDHDIDYKDDDDK) between amino acid positions Met-90 and Asp-91 in the IL-4Rα coding region of pME18s-IL4Rα using PCR. A series of IL-4Rα mutants were generated by PCR-based site-directed mutagenesis using FLAG-IL-4Rα as a template. FLAG-IL-4Rαd379, FLAG-IL-4Rαd399, FLAG-IL-4Rαd435, FLAG-IL-4Rαd400–418, FLAG-IL-4Rαd400–436, FLAG-IL-4RαmH, and FLAG-IL-4RαmA were IL-4Rα mutants with C-terminal truncations at positions 379, 399, and 435, deleted regions at positions 400–418 and 400–436, or mutations at positions 410–415 (^{410}LFLDLL/AAADAA^{415}) and 372–380 (^{372}EEEEVEEE/AAAAVAAA^{380}), respectively. Expression vectors containing FLAG-tagged wild-type IL-2Rβ (FLAG-IL-2Rβ) and its derivative mutants FLAG-IL-2Rβd268–348 and FLAG-IL-2Rβd349–410 were used (23). Additional IL-2Rβ mutants were created by PCR using FLAG-IL-2Rβ as a template. FLAG-IL-2RβmH1, FLAG-IL-2RβmH2, FLAG-IL-2RβmH3, FLAG-IL-2RβmA, and FLAG-IL-2RβmY were IL-2Rβ mutants with mutations at positions 336-338 (^{336}LLL/AAA^{338}), 365–369 (^{365}FFFHL/AAAHA^{369}), 407–411 (^{407}PLQPL/AAQAA^{411}), 389–394 (^{389}EEDPDE/AAAPAA^{394}) and 364–367 (^{364}YFFF/AFFF^{367}), respectively. pSRB5 is a human IL-2Rβ expression vector (24). Nontagged pME18s-IL-4RαmH and pSRβmH2 were also constructed by PCR using plasmids pME18s-IL4Rα and pSRβ5, respectively, as templates. pMXs-IL-4Rα, pMXs-IL-2Rα, and pMXs-IL-2Rγc were constructed by insertion of human IL-4Rα, IL-2Rα, and IL-2Rγc cDNAs, respectively, into a Moloney murine leukemia virus-derived vector, pMXs. pMXs-IL-2Rα-β269–551 and pMXs-IL-2Rα-β365–369 were generated by inserting the cytoplasmic tail (residues 269–551) and hydrophobic amino acid cluster (residues 365–369), respectively, of human IL-2Rβ at the C terminus of IL-2Rα. pMXsβ constructed by the insertion of human IL-2Rβ into pMXs was used (23). pMXsβmHP2 and pMXs-IL-4RαmH were created by PCR-based site-directed mutagenesis using pMXsβ and pMXs-IL-4Rα, respectively, as templates. pcDNA3-HA-ubiquitin was generously provided by K. Miyazono (The University of Tokyo, Tokyo). All constructs were sequenced with an ABI PRISM 3100 Genetic

Analyzer (Applied Biosystems) to verify the amino acid changes.

Cell Lines—HEK293T cells and mouse embryonic fibroblast (MEF) cells were maintained in DMEM supplemented with 10% fetal bovine serum (FBS) and antibiotics. MEFβ, MEFβ-mH2, MEF-IL4Rα, and MEF-IL4Rα-mH were stable cell clones expressing wild-type IL-2Rβ, IL-2RβmH2 mutant, wild-type IL-4Rα, and IL-4RαmH mutant, respectively. To introduce these genes into MEF cells, we used a pMXs retrovirus vector system (kindly provided by T. Kitamura, The University of Tokyo) and obtained single clones by the limiting dilution method. The mouse IL-3-dependent pro-B cell line BAF-B03 was maintained in RPMI 1640 medium supplemented with 10% FBS, 10% conditioned medium derived from WEHI-3 cell line cultures (as a source of IL-3), 50 μM 2-mercaptoethanol, and antibiotics. BAFβ, BAFβ-mH2, BAF-IL-4Rα, and BAF-IL-4Rα-mH were stable cell clones expressing wild-type IL-2Rβ, IL-2RβmH2 mutant, wild-type IL-4Rα, and IL-4RαmH mutant, respectively. Each gene and a hygromycin-resistance gene were co-introduced by electroporation into BAF-B03 cells, and positive clones were selected by their hygromycin resistance and the limiting dilution method.

Flow Cytometry—Cell surface marker expressions were examined by flow cytometry. Cells (1 $\times$ 10^6) were incubated with 10% FBS in phosphate-buffered saline (PBS) for 30 min on ice and then incubated with an anti-IL-2Rβ monoclonal antibody (TU11) (25) or anti-IL-4Rα monoclonal antibody (MAB230) (R&D Systems) for 30 min on ice. After three washes with PBS, the cells were incubated with a FITC-conjugated secondary antibody (MP Biomedicals) for 30 min on ice. After washing, the cells were fixed with 1% paraformaldehyde in PBS before analysis using a FACSCalibur (BD Biosciences).

Immunoprecipitation and Immunoblotting—Immunoprecipitation and immunoblotting were carried out as described previously (14). Briefly, HEK293T cells (1 $\times$ 10^6) were transfected with 3 μg of each vector using a calcium phosphate precipitation method and then lysed with Nonidet P-40 cell extraction buffer (1% Nonidet P-40, 20 mM Tris-HCl, pH 7.5, 150 mM NaCl, 1 mM EDTA, 1 mM Na$_3$VO$_4$, 2.5 mM sodium pyrophosphate, 1 mM β-glycerol phosphate, and 1 mM aprotinin). After preclearing, the lysates were immunoprecipitated with various antibodies immobilized on Protein A-Sepharose beads (GE Healthcare) at 4 °C for 1 h. The immunoprecipitates were extensively washed with a buffer (1% Nonidet P-40, 20 mM Tris-HCl, pH 7.5, 500 mM NaCl, 1 mM EDTA, 1 mM Na$_3$VO$_4$, 2.5 mM sodium pyrophosphate, 1 mM β-glycerol phosphate), boiled in SDS sample buffer, separated by SDS-PAGE, and transferred onto Immobilon-P membranes (Millipore). After blocking with 5% skim milk and 0.1% Tween 20 in Tris-buffered saline, the membranes were incubated with various primary antibodies at room temperature for 1 h, washed, and incubated with horse-radish-peroxidase-conjugated secondary antibodies (Cell Signaling Technology) at room temperature for 1 h. After a thorough washing, the positive signals were visualized using the Immobilon^{TM} Western substrate (Millipore). The primary antibodies utilized were: rabbit anti-HA, anti-IL-2Rβ (C20), anti-IL-4Rα (C20), rabbit anti-STAT5 (C17), and rabbit anti-phospho-STAT6 (Y641) antibodies (Santa Cruz Biotechnology,

Inc.), rabbit anti-STAT6 antibody and mouse anti-phosphotyrosine antibody (PY100) (Cell Signaling Technology), mouse anti-FLAG monoclonal antibody (M2) (Sigma), rabbit anti-phospho-STAT5 antibody (EPITOMICS), and rat anti-Hrs monoclonal antibody (Imos-1) (14).

Immunofluorescence Microscopy and Immunostaining— Cells grown on coverslips were fixed with 3% paraformaldehyde in PBS for 15 min at room temperature, permeabilized with 0.1% Triton X-100 in PBS for 10 min at room temperature or iced methanol for 5 min on ice, and incubated with 10% FBS in PBS for 30 min to block nonspecific antibody binding. For immunostaining, the cells were incubated with various primary antibodies at 30 °C for 1 h, washed 3 times with PBS, and incubated with appropriate secondary antibodies (anti-rabbit, anti-mouse, and anti-rat IgG antibodies conjugated with Alexa 488, Alexa 594, and FITC, respectively (Molecular Probes)) at 30 °C for 1 h. The coverslips were washed 5 times with PBS and mounted on glass slides with glycerol containing 0.1% *p*-phenylenediamine. Fluorescence images were captured using a confocal microscope (TCS SP2 (Leica) or LSM EXCITER (Carl Zeiss)). The primary antibodies utilized were: rabbit anti-IL-2Rβ antibody (C20), rabbit anti-IL-4Rα antibody (C20), mouse anti-IL-2Rβ antibody (TU11), mouse anti-IL-4Rα antibody (MAB230), rabbit anti-Hrs antibody (14), rat anti-mouse LAMP1 monoclonal antibody (1D4B), and rat anti-mouse transferrin receptor monoclonal antibody (R17217.1.4) (Santa Cruz Biotechnology Inc.); mouse anti-IL-2Rα antibody (H-31) (26), rat anti-IL-2Rγc antibody (TUGh4) (27), and mouse anti-lysobisphosphatidic acid (LBPA) monoclonal antibody (generously provided by T. Kobayashi, RIKEN Advanced Science Institute, Saitama, Japan).

GST Pulldown Assay—A His-tagged Hrs (His-Hrs) expression vector was constructed by insertion of wild-type Hrs into pCOLD® (TaKaRa). GST-tagged IL-2Rβ (GST-IL-2Rβ_{cy}) and IL-4Rα (GST-IL-4Rα_{cy}) expression vectors were generated by ligating the cytoplasmic tails of IL-2Rβ (amino acids 296–551) and IL-4Rα (amino acids 257–825), respectively, into pGEX-4T-1 (GE Healthcare). GST-IL-2Rβ_{cy}mH2 and GST-IL-4Rα_{cy}mH were created by PCR using GST-IL-2Rβ_{cy} and GST-IL-4Rα_{cy}, respectively, as templates. The BL21 strain of *Escherichia coli* was used to express the proteins, and the His-Hrs and GST fusion proteins were purified using nickel-nitrilotriacetic acid-agarose (Qiagen) and glutathione-Sepharose 4B beads (GE Healthcare), respectively. To investigate the interactions between Hrs and IL-2Rβ or IL-4Rα *in vitro*, glutathione-Sepharose 4B beads containing the immobilized GST fusion proteins were incubated with His-Hrs in a buffer (1% Nonidet P-40, 50 mM Hepes, pH 7.4, 150 mM NaCl, 0.1 mM EDTA, 1 mM PMSF) at 30 °C for 15 min. The beads were washed 3 times with washing buffer (1% Nonidet P-40, 50 mM Hepes, pH 7.4, 500 mM NaCl, 0.1 mM EDTA), and the bound proteins were analyzed by immunoblotting with an anti-His monoclonal antibody (Cell Signaling Technology).

Internalization and Degradation Assay—Anti-IL-2Rβ antibody (TU-11) and anti-IL-4Rα antibody (MAB230) were radiolabeled with Na^{125}I (MP Biomedicals) by the chloramine-T method. Recombinant IL-2 (Shionogi Co.) and recombinant IL-4 (PeproTech) were radiolabeled with Na^{125}I using a modi-

fied iodogen method (28). The specific activities of ^{125}I-TU-11, ^{125}I-MAB230, ^{125}I-IL-2, and ^{125}I-IL-4 were 4.8×10^6, 4.7×10^6, 2.0×10^6, and 9.5×10^5 dpm/pmol, respectively. For internalization assays, cells (2×10^6) were incubated with PBS, 10% FBS containing an ^{125}I-labeled antibody or ligand at 0 °C for 15 min. The cells were then washed 3 times with PBS, resuspended in RPMI/10% FBS, and incubated at 37 °C in a 5% CO$_2$ incubator for specified times. After centrifugation of the cell suspensions, the culture supernatants were collected, and the cell pellets were treated with chilled glycine buffer (200 mM glycine, pH 2.2, 150 mM NaCl) on ice for 10 min. The radioactivities of the culture supernatant fractions, acid-removable glycine buffer fractions, and acid-unremovable cell precipitates were counted. For degradation assays, cells (2×10^6) were incubated with PBS, 10% FBS containing an ^{125}I-labeled antibody or ligand at 0 °C for 15 min and washed with a cross-linking buffer (PBS containing 1 mM MgCl$_2$, pH 8.3). To cross-link cell surface receptors with the ^{125}I-labeled components, the cells were incubated with 300 μM dithiobis(sulfosuccinimidylpropionate) (DTSSP; Thermo Fisher Scientific, Inc.) in the cross-linking buffer on ice for 10 min. The cells were then washed twice with PBS containing 50 mM Tris-HCl, pH 7.4, resuspended in RPMI, 10% FBS, and incubated at 37 °C in a 5% CO$_2$ incubator for the specified times. After centrifugation of the cell suspensions, the radioactivities of the culture supernatants and cell pellets were counted. The culture supernatants were further treated with 10% trichloroacetic acid (TCA) and incubated at 4 °C overnight. The radioactivities of the TCA-soluble fractions were counted.

Colocalization Image Analysis—Quantification of colocalization images captured with an LSM EXCITER confocal microscope (Carl Zeiss) was carried out using the ZEN2009 software (Carl Zeiss). Confocal images of single cells were captured randomly (carefully avoiding signal saturation), and each image was redistributed into 0–255 intensity levels. The fluorescence signals of more than 100 intensity levels per pixel were counted (29). The primary antibodies utilized were: rabbit anti-IL-2Rβ antibody (C20), rabbit anti-IL-4Rα antibody (C20), rat anti-mouse LAMP1 monoclonal antibody (1D4B), and mouse anti-LBPA monoclonal antibody.

RESULTS

UIM-deleted Hrs Interacts with IL-4Rα—We previously found that IL-2Rβ interacts with Hrs in a ubiquitin-independent manner (23). Thus, analyses of the cytoplasmic regions of both IL-2Rβ and another cytokine receptor that interacts with Hrs in the same manner will contribute to the identification of an Hrs binding motif in the ubiquitin-independent Hrs binding regions of the receptors. The receptors for IL-2, IL-4, IL-7, IL-9, IL-15, and IL-21 utilize the IL-2Rγc chain as an essential subunit (14, 22), suggesting the possibility that these receptors may have similar biological and biochemical characters for endosomal sorting. Therefore, we selected the IL-4 receptor α chain (IL-4Rα) and examined this possibility. The UIM domain of Hrs is necessary for ubiquitin binding and sorting of ubiquitylated cargo proteins into the MVB pathway (16, 20, 21). We previously reported that a UIM-deleted Hrs mutant can bind to IL-2Rβ (23). Accordingly, to examine
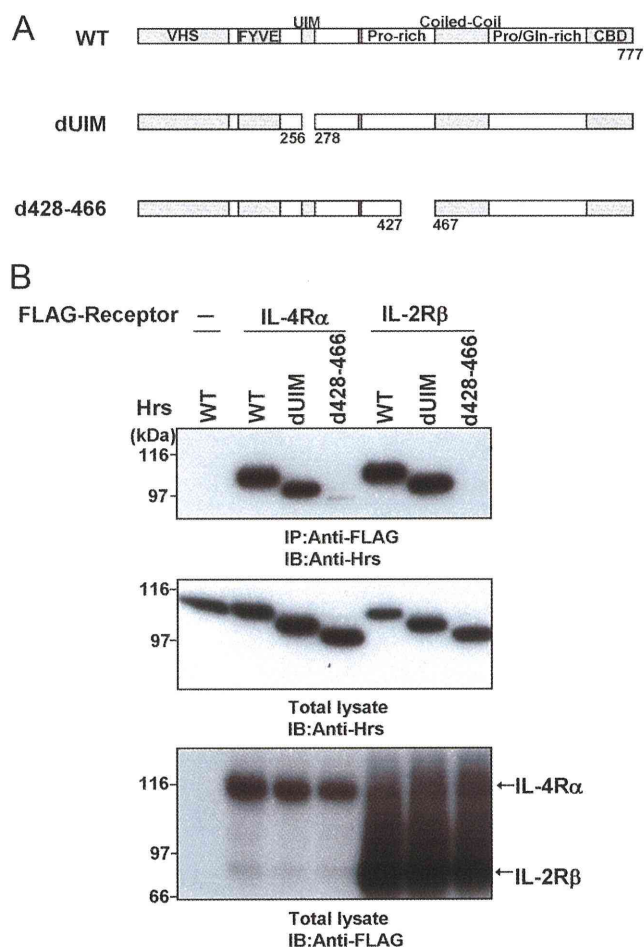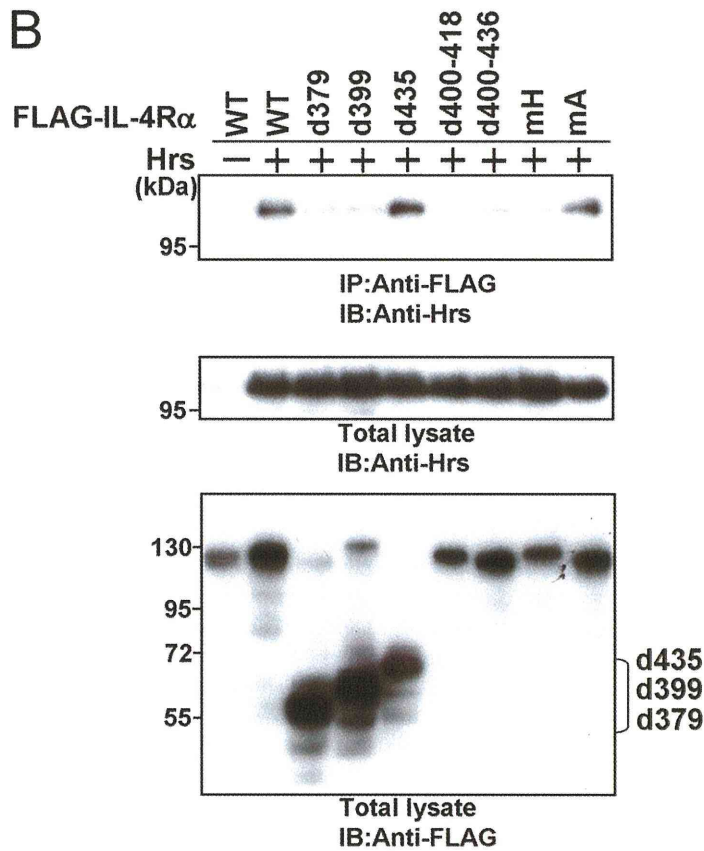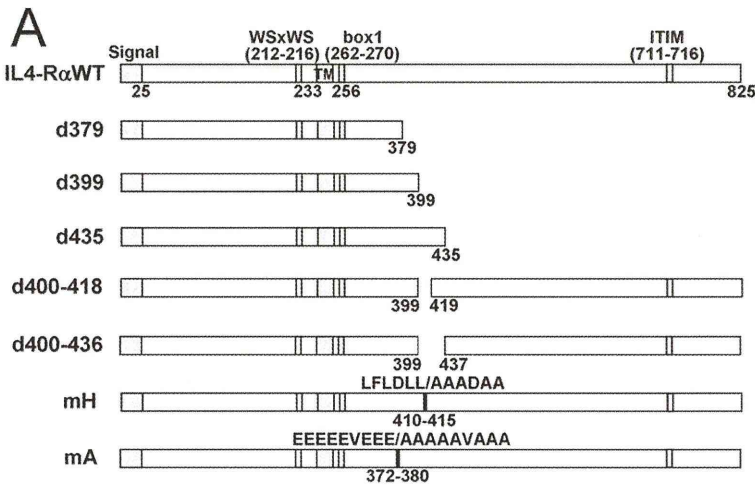
FIGURE 1. **The UIM domain of Hrs is dispensable for the interaction between Hrs and IL-4Rα.** *A,* structures of wild-type Hrs and its mutants are shown. The Vps27-Hrs-STAM (*VHS*), Fab1-YGL023-Vps27-EEA1 (*FYVE*), ubiquitin interacting motif (*UIM*), proline (*Pro*)-rich region, coiled-coil, proline/glutamine (*Pro/Gln*)-rich region, and clathrin binding domain (*CBD*) are indicated. *B,* HEK293T cells (1 × 10⁶) were cotransfected with 3 μg of wild-type FLAG-IL-2Rβ, wild-type FLAG-IL-4Rα, or empty vector and 3 μg of wild-type Hrs or its mutants. Aliquots (400 μg) of the cell lysates were immunoprecipitated with an anti-FLAG monoclonal antibody and immunoblotted with an anti-Hrs monoclonal antibody (*top panel*). The expression levels of Hrs and FLAG-tagged receptors in total lysates of the transfected HEK293T cells were examined by immunoblotting with an anti-Hrs monoclonal antibody and anti-FLAG monoclonal antibody, respectively. *Total lysate,* aliquots (10 μg) of the lysates were immunoblotted with an anti-Hrs antibody (*middle panel*) or anti-FLAG monoclonal antibody (*lower panel*). *IP,* immunoprecipitation; *IB,* immunoblotting.

whether the UIM-deleted mutant can bind to IL-4Rα, we performed coimmunoprecipitation assays. Human embryonic kidney-derived (HEK) 293T cells were transiently transfected with FLAG-tagged IL-4Rα or IL-2Rβ and Hrs expression vectors (Fig. 1A). Lysates of the HEK293T cells were immunoprecipitated with an anti-FLAG antibody and immunoblotted with an anti-Hrs antibody. Similar to IL-2Rβ, wild-type Hrs and the UIM-deleted mutant were clearly coimmunoprecipitated with IL-4Rα (Fig. 1B). We also previously reported that amino acids 428–466 of Hrs are a key domain for its ubiquitin-independent binding to IL-2Rβ (23). The association of Hrs lacking amino acids 428–466 with IL-4Rα was drastically reduced, similar to the

case for IL-2Rβ (Fig. 1B). These results suggest that the manner of IL-4Rα binding to Hrs is similar to that of IL-2Rβ.

Hrs Binding Motif in IL-4Rα and IL-2Rβ—To define the region of IL-4Rα required for its interaction with Hrs, we constructed IL-4Rα mutants truncated at amino acids 379, 399, and 435 (Fig. 2A) and investigated their binding abilities toward Hrs by coimmunoprecipitation analyses (Fig. 2B). Hrs binding was clearly detected in the lysates of HEK293T cells transfected with the IL-4Rα mutant comprising amino acids 1–435 (d435) but was markedly reduced after coimmunoprecipitation with the mutants comprising amino acids 1–379 (d379) and 1–399 (d399). These observations suggested that amino acids 400–435 include an important region for Hrs binding. Further experiments revealed that deletion mutants lacking amino acids 400–418 (d400–418) and 400–436 (d400–436) (Fig. 2A) were hardly able to bind to Hrs (Fig. 2B). These findings suggest the possibility that there is an amino acid cluster or motif for Hrs binding within amino acids 400–418. We then aligned the amino acid sequences of human, bovine, swine, horse, rat, and mouse IL-4Rα and found a hydrophobic amino acid cluster within amino acids 400–418 (Fig. 2C). In addition, we detected an acidic cluster (amino acids 372–380) (Fig. 2C) that is often identified as a binding motif between proteins during endosomal sorting (1). We constructed an mH mutant in which the hydrophobic amino acids were substituted with alanine within residues 410–415 and an mA mutant in which the acidic amino acids were substituted with alanine within residues 372–380. Although significant binding was observed between Hrs and the mA mutant, an association of the mH mutant with Hrs was barely detectable (Fig. 2B). Accordingly, we aligned the amino acid sequences of human and other mammalian IL-2Rβ proteins and found three hydrophobic clusters and one acidic amino acid cluster (Fig. 3A). We then substituted the hydrophobic amino acids in the three hydrophobic amino acid clusters in IL-2Rβ with alanine and generated the mH1, mH2, and mH3 mutants with mutations located at residues 336–338, 365–369, and 407–411, respectively (Fig. 3B). In addition, we substituted the acidic amino acids of the Hrs binding region in IL-2Rβ with alanine and generated the mA mutant with mutations located at residues 389–394 (Fig. 3B). The deletion mutant lacking residues 349–410 was previously reported as an IL-2Rβ mutant lacking Hrs binding ability (23). The mH2 and d349–410 mutants were completely unable to bind to Hrs, although the mH1, mH3, and mA mutants strongly bound to Hrs (Fig. 3C). Thus, one of the three hydrophobic amino acid clusters is involved in the interactions between these proteins, suggesting that a steric structure beside the cluster may play an important part in Hrs binding. We further generated an mY mutant in which tyrosine residue 364 was substituted with alanine, as the tyrosine at residue 364 is located at the N-terminal side of amino acids 365–369 (mutated area in the mH2 mutant) and corresponds to a tyrosine-based signal (YXXφ (φ indicates a residue with bulky hydrophobic side chains)) involved in endosomal sorting (Fig. 3, A and B). The mY mutant as well as wild-type IL-2Rβ bound to Hrs (Fig. 3C). These findings indicate that tyrosine residue 364 and the acidic amino acid cluster are not essential for Hrs binding.

A

IL4-RαWT

d379

d399

d435

d400-418

d400-436

mH — LFLDLL/AAADAA — 410-415

mA — EEEEEVEEE/AAAAAVAAA — 372-380

B

FLAG-IL-4Rα: WT, WT, d379, d399, d435, d400-418, d400-436, mH, mA

Hrs: −, +, +, +, +, +, +, +, +

IP:Anti-FLAG
IB:Anti-Hrs

Total lysate
IB:Anti-Hrs

d435
d399
d379

Total lysate
IB:Anti-FLAG

C

Acidic cluster — Hydrophobic cluster

```
Human   341- WCPVEISKTVLWPE---SISVVRCVELFEAPVEQEEEEEVEEEKGSFCASPESSRD-DFQEGREGIVARLTESLFLDLLGEENGG--------  -421
Bovine  344- WCPVEVSKTILRPE---SISVVRCVELFEAQVE-KEEEEVEEDKGSFCPSPENSGG-LFQEGREDIAARLTESLFLHLLRDETGG--------  -423
Swine   349- WRPVEVSKTILWPE---SISVVRCVELFEAQVE-NEEEEEEEDKGSFCPSPENSGG-SFQEGREGIAARLTESLFLDLLGDESGAFSPQGMG  -435
Horse   340- WHTVEVNHTILRPE---IISVVPCVELCEAQVE-SEEEEVEEDRGSFCPSPESSGS-GFQEGREGVAARLTESLFLGLLGAENGA--------  -419
Rat     341- WYPAEVSRTVLWPENVHVSVVRCVELFEAPVQNVEEEEDEMVKGDLSMSPENSGG-GFQESQADIMARLTENLFSDLLGAENGG--------  -423
Mouse   342- WCPMEVSRTVLWPENVSVSVVRCVELFEAPVQNVEEEEDEIVKEDLSMSPENSGGCGFQESQADIMARLREHLFSDLLEAENGG--------  -425
```

VOLUME 286•NUMBER 17•APRIL 29, 2011
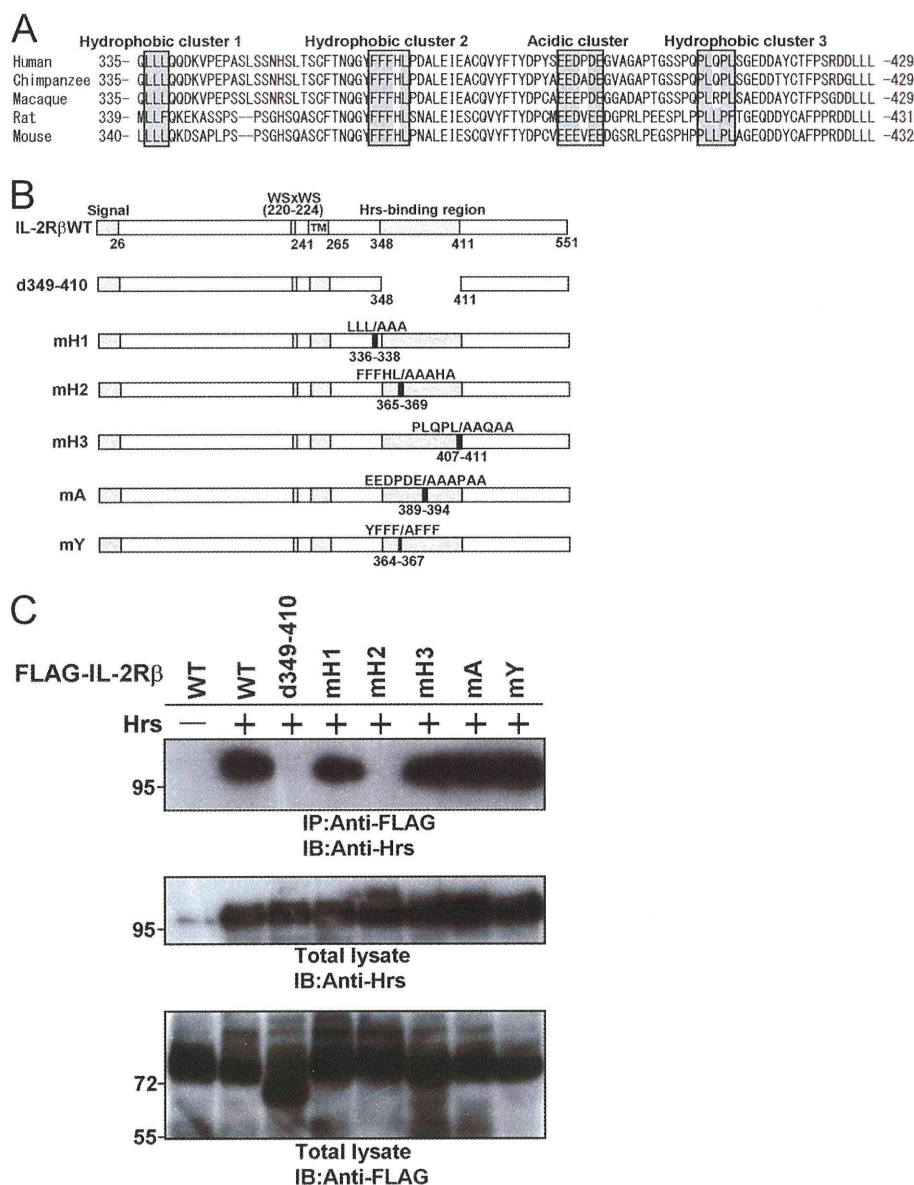
FIGURE 3. **A hydrophobic amino acid cluster in the cytoplasmic tail of IL-2Rβ is required for Hrs binding.** *A*, multiple alignment of the Hrs binding regions of human, chimpanzee, macaque, rat, and mouse IL-2Rβ is shown. The regions defined as acidic and hydrophobic clusters are *boxed*. *B*, shown are structures of wild-type IL-2Rβ and its mutants. The signal sequence, WS*X*WS motif, transmembrane region (*TM*), and Hrs binding region are indicated. *C*, HEK293T cells (1 × 10⁶) were cotransfected with 3 μg of FLAG-tagged wild-type IL-2Rβ or its mutants and 3 μg of wild-type Hrs or empty vector. Aliquots (400 μg) of the cell lysates were immunoprecipitated with an anti-FLAG monoclonal antibody and immunoblotted with an anti-Hrs monoclonal antibody (*top panel*). The expression levels of Hrs and IL-2Rβ were examined by immunoblotting with an anti-Hrs monoclonal antibody and anti-FLAG monoclonal antibody, respectively. *Total lysate*, aliquots (10 μg) of the lysates were immunoblotted with an anti-Hrs monoclonal antibody (*middle panel*) or anti-FLAG monoclonal antibody (*lower panel*). *IP*, immunoprecipitation; *IB*, immunoblotting.

The Hydrophobic Amino Acid Cluster Is Involved in Direct Interactions between Hrs and IL-4Rα or IL-2Rβ—We previously identified a direct interaction between bacterially expressed IL-2Rβ and Hrs in GST pulldown assays (23). To explore whether the hydrophobic amino acid cluster is involved in the direct association with Hrs, we prepared purified protein

FIGURE 2. **A hydrophobic amino acid cluster in the cytoplasmic tail of IL-4Rα is required for Hrs binding.** *A*, structures of wild-type IL-4Rα and its mutants are shown. The signal sequence, WS*X*WS (tryptophan, serine, any amino acid, tryptophan, serine) motif, transmembrane region (*TM*), box1 motif, and immunoreceptor tyrosine-based inhibitory motif (*ITIM*) are indicated. *B*, HEK293T cells (1 × 10⁶) were cotransfected with 3 μg of FLAG-tagged wild-type IL-4Rα or its mutants and 3 μg of wild-type Hrs or empty vector. Aliquots (400 μg) of the cell lysates were immunoprecipitated with an anti-FLAG monoclonal antibody and immunoblotted with an anti-Hrs monoclonal antibody (*top panel*). The expression levels of Hrs and IL-4Rα were examined by immunoblotting with an anti-Hrs monoclonal antibody and anti-FLAG monoclonal antibody, respectively. *Total lysate*, aliquots (10 μg) of the lysates were immunoblotted with an anti-Hrs monoclonal antibody (*middle panel*) or anti-FLAG monoclonal antibody (*lower panel*). *IP*, immunoprecipitation; *IB*, immunoblotting. *C*, multiple alignment of the Hrs binding regions of human, bovine, swine, horse, rat, and mouse IL-4Rα is shown. The regions defined as acidic or hydrophobic clusters are *boxed*.

extracts from *E. coli* expressing His-tagged Hrs, GST-tagged IL-2Rβ, and GST-tagged IL-2Rβ with the hydrophobic amino acid cluster substituted with alanine (IL-2RβmH2) or GST-tagged IL-4Rα or GST-tagged IL-4Rα with the hydrophobic amino acid cluster substituted with alanine (IL-4RαmH). The GST-tagged fusion proteins were immobilized on glutathione-Sepharose beads, and each fusion protein was incubated with His-tagged Hrs. The beads were washed, and bound material was immunoblotted with an anti-His antibody. Wild-type IL-2Rβ and IL-4Rα associated with His-tagged Hrs, whereas IL-2RβmH2, IL-4RαmH, and GST alone did not (Fig. 4A). These results suggested that the hydrophobic amino acid clusters in IL-2Rβ and IL-4Rα are involved in their Hrs binding abilities in a ubiquitylation-independent manner. Next, we examined whether the hydrophobic amino acid cluster affects the ubiquitylation of the receptors. HEK293T cells were transfected with HA-tagged ubiquitin and wild-type or mutant receptors as shown in Fig. 4C. Although the IL-2Rβ mutant lacking residues 268–348, in which all the lysine residues of the cytoplasmic tail are located, was hardly ubiquitylated, IL-2RβmH2 and IL-4RαmH were similarly ubiquitylated to the wild-type receptors (Fig. 4, B and C). These observations indicated that the ubiquitylation of the receptors is not affected by the issue of whether Hrs interacts with the receptors through the hydrophobic amino acid cluster.

The Hydrophobic Amino Acid Clusters of IL-2Rβ and IL-4Rα Are Required for Endosomal Sorting to Late Endosomes—We previously examined the endocytic intracellular localization of IL-2Rβ by confocal microscopy using an anti-IL-2Rβ antibody together with antibodies against the early endosome marker EEA1 (or Hrs) or late endosome/lysosome marker LAMP1. The experiments revealed that IL-2Rβ is localized to LAMP1-positive compartments and rarely found in EEA1-positive and Hrs-positive compartments under steady-state conditions (23). In addition, a kinetics study on IL-2Rβ endosomal sorting revealed that IL-2Rβ is delivered to LAMP1-positive compartments through Hrs-positive compartments (23). Therefore, we investigated the effects of the hydrophobic amino acid cluster on the localizations of IL-2Rβ and IL-4Rα. cDNAs encoding the IL-2Rβ mutant with the hydrophobic amino acid cluster substituted with alanine and wild-type IL-2Rβ were introduced into a MEF cell line to generate MEFβ-mH2 and MEFβ cells, respectively. MEF-IL-4Rα-mH and MEF-IL-4Rα cells were similarly established as MEF cells expressing IL-4RαmH and IL-4Rα, respectively. FACS and immunoblotting analyses indicated that there were no significant differences between the amounts of the wild-type and mutant receptors on the cell surfaces or in the intracellular expressions of the transfectants (Fig. 5, A and B). Although wild-type IL-2Rβ in MEFβ cells and IL-4Rα in MEF-IL-4Rα cells were localized to LAMP1-positive compartments, the mutant IL-2Rβ in MEFβ-mH2 cells and mutant IL-4Rα in MEF-IL-4Rα-mH cells were localized to punctate structures in the cytoplasm rather than to LAMP1-positive compartments (Fig. 5, C and D). Taken together with the data shown in Fig. 4A, these findings suggest that the hydrophobic amino acid clusters involved in the interactions between Hrs and the receptors play a key role in the sorting to LAMP1-positive compartments.
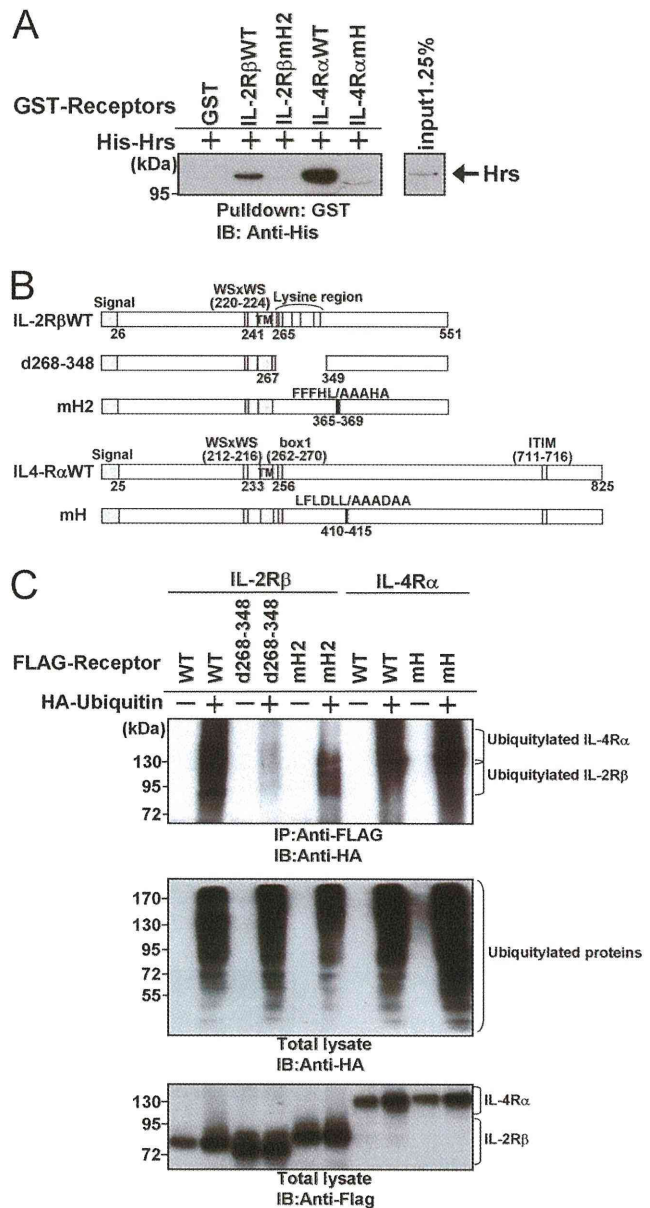
FIGURE 4. **Hrs directly associates with the cytokine receptors IL-2Rβ and IL-4Rα by recognizing the hydrophobic amino acid cluster in a ubiquitin-independent manner.** *A*, glutathione-Sepharose beads containing immobilized GST, GST-fused cytoplasmic tail fragment of IL-2Rβ (GST-IL-2Rβ$_{cy}$WT or GST-IL-2Rβ$_{cy}$mH2), or GST-fused cytoplasmic tail fragment of IL-4Rα (GST-IL-4Rα$_{cy}$WT or GST-IL-4Rα$_{cy}$mH) were incubated with His-tagged Hrs. The bound proteins were separated by SDS-PAGE and analyzed by immunoblotting with an anti-His tag antibody. The input control of His-Hrs is shown in the *right panel*. *B*, structures of the IL-2Rβ and IL-4Rα mutants used in the receptor ubiquitylation assays are shown. *C*, HEK293T cells were cotransfected with 2 μg of HA-ubiquitin or empty vector and 2 μg of FLAG-IL-2Rβ, FLAG-IL-2Rβd268–348, FLAG-IL-2RβmH2, FLAG-IL-4Rα, or FLAG-IL-4RαmH. Aliquots (200 μg) of the cell lysates were immunoprecipitated with an anti-FLAG monoclonal antibody and immunoblotted with an anti-HA monoclonal antibody (*top panel*). The expression levels of the receptors (IL-2Rβ and IL-4Rα) and ubiquitylated total proteins were examined by immunoblotting with an anti-FLAG monoclonal antibody and anti-HA monoclonal antibody, respectively. *Total lysate*, aliquots (10 μg) of the lysates were immunoblotted with an anti-HA antibody (*middle panel*) or anti-FLAG antibody (*lower panel*). *IP*, immunoprecipitation; *IB*, immunoblotting.
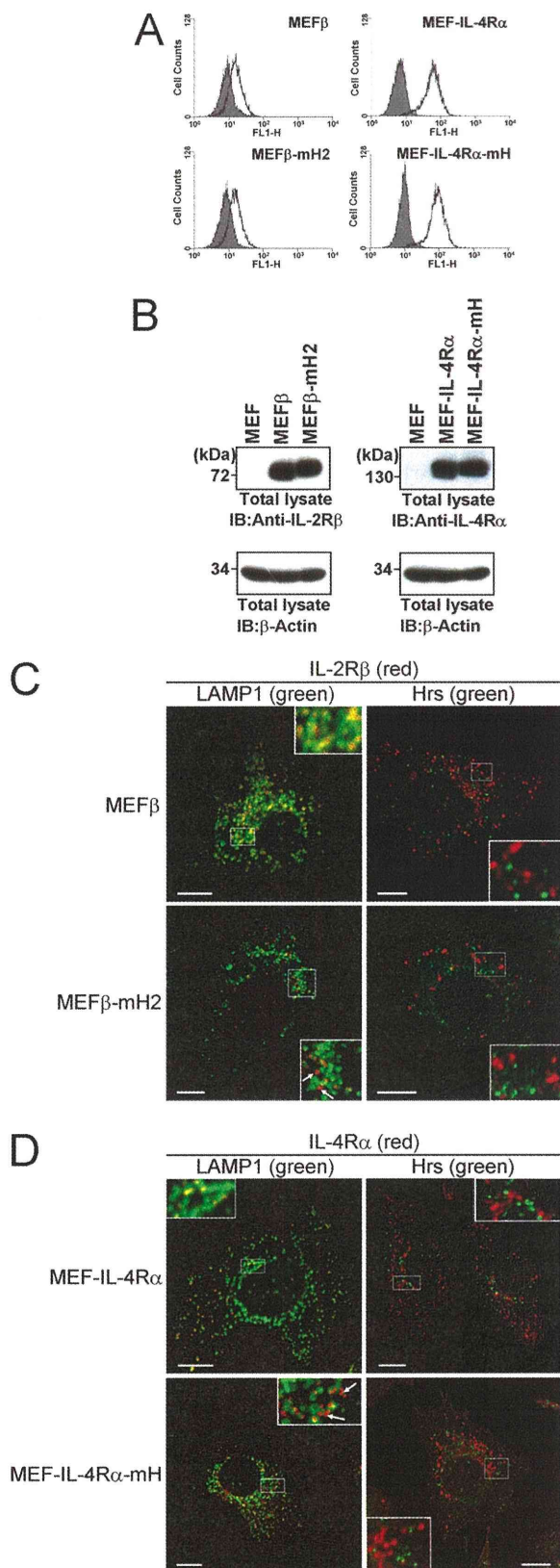
FIGURE 5. **Effects of the hydrophobic amino acid clusters in IL-2Rβ and IL-4Rα on their late-endosomal localizations.** *A*, the IL-2Rβ and IL-4Rα expression levels on the surface of MEF transfectants were examined by flow

In a previous kinetics study on IL-2Rβ endosomal sorting, IL-2Rβ$_{d349-410}$ lacking amino acids 349–410, which include the hydrophobic amino acid cluster (residues 365–369), was observed in Hrs-positive compartments at 10 min after the receptor internalization and had departed from these compartments at 30 min (23). However, the sorting of IL-2Rβ$_{d349-410}$ to LAMP1-positive compartments was largely impaired (23). Therefore, we investigated whether IL-4RαmH and IL-2RβmH2 are delivered to the punctate structures shown in Fig. 5, *C* and *D*, through Hrs-positive compartments. MEFβ-mH2 and MEFβ cells were incubated at 0 °C to suppress the receptor internalization and treated with the anti-IL-2Rβ antibody TU11. The receptors were covalently linked to TU11 by incubation with DTSSP as a chemical cross-linker. Next, the cells were incubated at 37 °C for the indicated times and analyzed by confocal microscopy. IL-2Rβ and IL-2RβmH2 were observed in Hrs-positive compartments at 10 min and had departed from these compartments at 60 min (Fig. 6A). At 120 min, a large proportion of IL-2Rβ had been delivered to LAMP1-positive compartments, whereas IL-2RβmH2 had been partially delivered to LAMP1-positive compartments (Fig. 6A). Similarly, IL-4Rα was delivered to LAMP1-positive compartments through Hrs-positive compartments, whereas blockade of IL-4RαmH transportation to the LAMP1-positive compartments was observed (Fig. 6B). These findings indicate that the hydrophobic amino acid clusters in these receptors play a key role in endosomal sorting of the receptors from early to late endosomes.

Subsequently, we examined whether the hydrophobic amino acid cluster introduced into a recycling receptor serves as the sorting signal to LAMP1-positive endosomes. We then constructed chimeric receptors of IL-2Rα, which is constitutively internalized and rapidly recycled back to the plasma membrane (30). The hydrophobic amino acid cluster (residues 365–369) or the cytoplasmic tail (residues 269–551) of IL-2Rβ was inserted at the C terminus of IL-2Rα (supplemental Fig. S1A). MEF cells transiently expressing wild-type IL-2Rα, the chimeric receptor including the residues 365–369 (IL-2Rα-β365–369), or the residues 269–551 (IL-2Rα-β269–551) were incubated at 0 °C and treated with the anti-IL-2Rα antibody H-31. Next, the cells were incubated at 37 °C for 120 min and analyzed by confocal microscopy. Although a large part of wild-type IL-2Rα was observed on the plasma membrane, IL-2Rα-β269–551, including the cytoplasmic tail of IL-2Rβ, was detected in LAMP1-positive compartments (supplemental Fig. S1B). On

cytometry. MEFβ, MEFβ-mH2, MEF-IL-4Rα, and MEF-IL-4Rα-mH cells were incubated with an anti-IL-2Rβ monoclonal antibody (TU11) or anti-IL-4Rα monoclonal antibody (MAB230) followed by a FITC-conjugated secondary antibody. *B*, the expression levels of IL-2Rβ and IL-4Rα in the indicated cells were examined by immunoblotting. Aliquots (15 μg) of the total lysates were immunoblotted with an anti-IL-2Rβ antibody (C20) or anti-IL-4Rα antibody (C20) (*upper panels*) or with an anti-β-actin antibody (*lower panels*). *C* and *D*, fluorescence images were observed using a confocal laser microscope. The indicated cells were grown on coverslips, fixed, and double-labeled with an anti-IL-2Rβ antibody (TU11) or anti-IL-4Rα antibody (MAB230) and an anti-LAMP1 monoclonal antibody or anti-Hrs antibody. Subsequently, the cells were incubated with fluorescently labeled secondary antibodies. Fairly large amounts of IL-2RβmH2 and IL-4RαmH are not sorted to LAMP1-positive compartments (*arrows*). *Scale bars*, 10 μm. *IB*, immunoblotting.

A

B
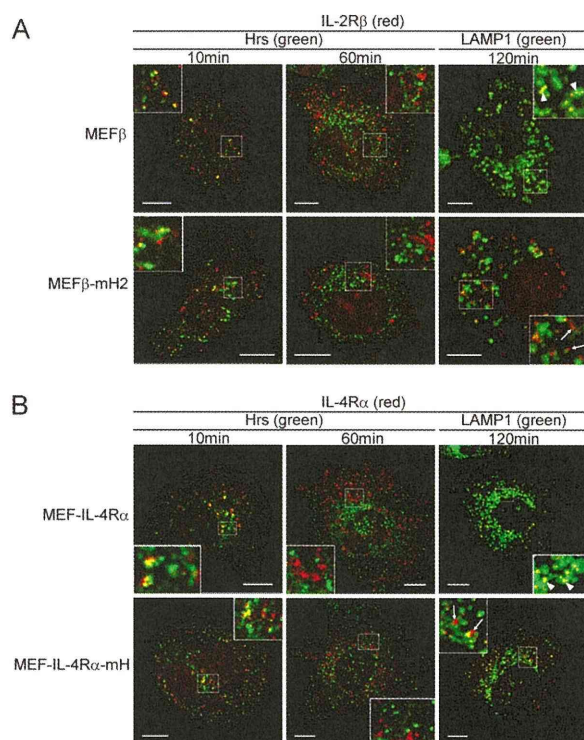
FIGURE 6. **Kinetics of the endosomal localizations of IL-2Rβ and IL-4Rα.** *A* and *B*, the indicated MEF transfectants were grown on coverslips, and the cell surface receptors were bound by an anti-IL-2Rβ antibody (TU11) or anti-IL-4Rα antibody (MAB230) at 0 °C followed by treatment with the chemical cross-linker DTSSP. The cells were cultured at 37 °C, fixed at the indicated times, and incubated with an anti-Hrs antibody or anti-LAMP1 monoclonal antibody. Fluorescence labeling was carried out for IL-2Rβ (*red*), IL-4Rα (*red*), Hrs (*green*), and LAMP1 (*green*). Large proportions of IL-2Rβ and IL-4Rα are delivered to LAMP1-positive compartments (*arrowheads*). In contrast, fairly large amounts of IL-2RβmH2 and IL-4RαmH are not delivered to LAMP1-positive compartments (*arrows*). *Scale bars*, 10 μm.

the other hand, IL-2Rα-β365–369, including the hydrophobic amino acid cluster of IL-2Rβ as well as wild-type IL-2Rα, was found on the plasma membrane, indicating that the other cytoplasmic region along with the hydrophobic amino acid cluster is also needed for the function as the sorting signal.

Involvement of the Hydrophobic Amino Acid Clusters in the Degradation of IL-2Rβ and IL-4Rα in BAF-B03 Transfectants— To analyze the internalization and degradation of IL-2RβmH2 and IL-4RαmH lacking the hydrophobic amino acid cluster required for Hrs binding, we used IL-2Rβ-deficient BAF-B03 cells expressing mouse IL-2Rα and IL-2Rγc. The mouse pro-B cell line BAF-B03 is an IL-3-dependent cell line, and its transfectants with human cytokine receptor genes (IL-2Rβ and IL-4Rα) have been used to analyze cytokine signal transduction (31, 32). cDNAs encoding the IL-2Rβ mutant with the hydrophobic amino acid cluster substituted with alanine and wild-type IL-2Rβ were introduced into BAF-B03 cells to generate BAFβ-mHP2 and BAFβ cells, respectively. BAF-IL-4Rα-mH and BAF-IL-4Rα cells were similarly established as BAF-B03 cells expressing IL-4RαmH and IL-4Rα, respectively. Using FACS analyses, we selected two types of cell clones; one expressing a higher amount of each receptor and the other expressing a lower amount of each receptor on the cell surface (supplemental Fig. S2, *A and B*). First, we examined the kinetics

of the receptor internalization in the transfectants. BAFβ clone 15, BAFβ clone 21, BAFβ-mH2 clone 10, and BAFβ-mHP2 clone 38 cells were incubated with ^{125}I-anti-IL-2Rβ antibody (TU11). TU11 does not block receptor assembly among the IL-2Rα, -β and, -γc chains (24). In addition, TU11 neither stimulates nor inhibits IL-2R-mediated cell growth (33). To evaluate the receptor internalization, the cells were collected at the indicated times (Fig. 7*A*). Treatment of the cells with 200 mM glycine buffer, pH 2.2, was used to distinguish the cell surface-bound ^{125}I-TU11 from the intracellular ^{125}I-TU11. The radioactivity of the cell surface-bound acid-removable ^{125}I-TU11 decreased rapidly (Fig. 7*Aa*) accompanied by a rapid increase in the radioactivity of intracellular acid-unremovable ^{125}I-TU11 (Fig. 7*Ab*), indicating that IL-2Rβ is constitutively internalized in the absence of the ligand, as previously reported (23). The kinetics of ^{125}I-TU11 internalization in BAFβ-mHP2 cells was similar to that in BAFβ cells, and the different levels of receptor expression in these clones had no effect on the kinetics (Fig. 7*A*). Similar to BAFβ cells, BAF-IL-4Rα clone 18, BAF-IL-4Rα clone 38, BAF-IL-4Rα-mH clone 2, and BAF-IL-4Rα-mH clone 48 cells were incubated with an ^{125}I-anti-IL-4Rα antibody, which blocks IL-4 binding to IL-4Rα, and then analyzed for the internalization of IL-4Rα. The kinetics of ^{125}I-conjugated anti-IL-4Rα antibody internalization in BAF-IL-4Rα-mH cells was similar to that in BAF-IL-4Rα cells (Fig. 7*B*), and the kinetics of the blocking-type anti-IL-4Rα antibody was similar to that of TU11 (Fig. 7, *A* and *B*). Subsequently, we evaluated the receptor degradation based on the amount of radioactivity released into the culture supernatants by the cells. The transfectants expressing IL-2Rβ and IL-4Rα were incubated with the ^{125}I-TU11 and ^{125}I-anti-IL-4Rα antibodies, respectively, and the receptors were covalently linked with the ^{125}I-TU11 or ^{125}I-anti-IL-4Rα antibodies using the chemical cross-linker DTSSP before the culture supernatants were collected at the indicated times (Fig. 7, *C* and *D*). The radioactivities in the culture supernatants increased (Fig. 7, *Ca* and *Da*), and the increases were quantitatively correlated with decreases in the cell-bound radioactivity (Fig. 7, *Cb* and *Db*). The radioactivity in the culture supernatants of BAFβ-mHP2 clones was apparently lower than that of BAFβ clones (Fig. 7*Ca*), and the radioactivity in the culture supernatants of BAF-IL-4Rα-mH clones was apparently lower than that of BAF-IL-4Rα clones (Fig. 7*Da*). Furthermore, we extracted the degraded short peptides from the culture supernatants by TCA precipitation and found lower amounts of degraded short peptides in the culture supernatants of BAFβ-mHP2 and BAF-IL-4Rα-mH cells compared with those in the culture supernatants of BAFβ and BAF-IL-4Rα cells, respectively (Fig. 7, *Cc* and *Dc*). Taken together, these findings indicate that the degradation rates of the mutant receptors with the hydrophobic amino acid clusters substituted with alanine are lower than those of the wild-type receptors.

As shown in Fig. 6, confocal microscopy analyses using MEFβ-mH2, MEFβ, MEF-IL-4Rα-mH, and MEF-IL-4Rα cells revealed that the sorting of IL-2RβmH2 and IL-4RαmH to LAMP1-positive compartments was partially impaired. Therefore, we used the MEF transfectants to investigate the receptor internalization and degradation. The kinetics of ^{125}I-TU11 internalization in MEFβ-mHP2 cells was the same as that in

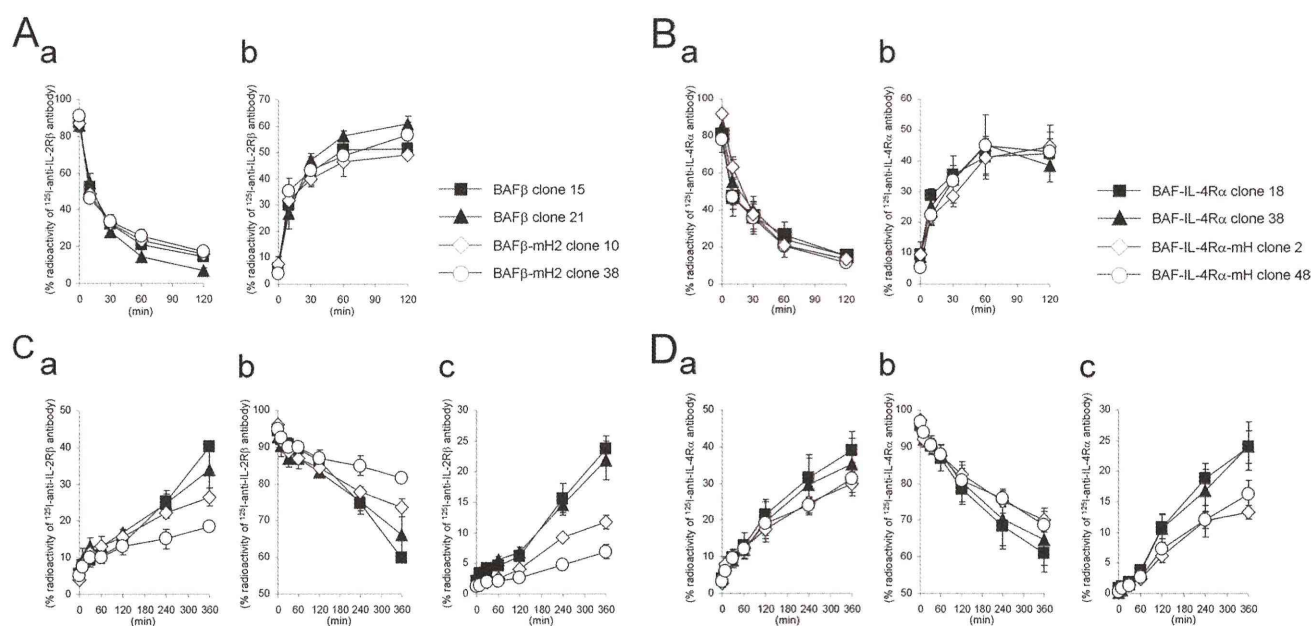FIGURE 7. **Internalization and degradation of IL-2Rβ and IL-4Rα in BAF-B03 transfectants.** *A* and *B*, shown is internalization of IL-2Rβ and IL-4Rα in the transfectants. BAF transfectants were incubated with ^{125}I-anti-IL-2Rβ antibody (TU11) or ^{125}I-anti-IL-4Rα antibody (MAB230) at 0 °C. The cells were then cultured at 37 °C and harvested at the indicated times. The radioactivities of the cell surface-bound acid-removable fractions (*a*) and intracellular acid-unremovable fractions (*b*) were counted. *C* and *D*, degradation of IL-2Rβ and IL-4Rα in the transfectants is shown. BAF transfectants were incubated with ^{125}I-anti-IL-2Rβ antibody or ^{125}I-anti-IL-4Rα antibody at 0 °C followed by treatment with the chemical cross-linker DTSSP. The cells were then cultured at 37 °C and harvested at the indicated times. The radioactivities of the culture supernatants (*a*), cell precipitate fractions (*b*), and TCA-soluble fractions of the culture supernatants (*c*) were counted. The values represent the means ± S.E. of three separate experiments.

MEFβ cells (supplemental Fig. S3*A*). In addition, the kinetics of ^{125}I-anti-IL-4Rα antibody internalization in MEF-IL-4Rα-mH cells was the same as that in MEF-IL-4Rα cells (supplemental Fig. S3*B*). Subsequently, however, the radioactivities in the culture supernatants of MEFβ-mHP2 and MEF-IL-4Rα-mH cells were apparently lower than those in the culture supernatants of MEFβ and MEF-IL-4Rα cells, respectively (supplemental Fig. S3, *C* and *D*), and the amounts of the degraded short peptides in the culture supernatants of MEFβ-mHP2 and MEF-IL-4Rα-mH cells were lower than those in the culture supernatants of MEFβ and MEF-IL-4Rα cells, respectively (supplemental Fig. S3, *Cc* and *Dc*). Therefore, the lower amounts of degraded short peptides observed for the mutant receptors may reflect a partial sorting of the mutant receptors to LAMP1-positive compartments.

Next, we examined the kinetics of the ligand degradation in the BAF-B03 transfectants. The transfectants expressing IL-2Rβ were incubated with ^{125}I-IL-2 and analyzed for IL-2 internalization. The radioactivity of the cell surface-bound acid-removable ^{125}I-IL-2 decreased rapidly (Fig. 8*Aa*) accompanied by a rapid increase in the radioactivity of intracellular acid-unremovable ^{125}I-IL-2 (Fig. 8*Ab*). The kinetics of ^{125}I-IL-2 internalization in BAFβ-mH2 cells was similar to that in BAFβ cells (Fig. 8*A*). Subsequently, we evaluated the ^{125}I-IL-2 degradation based on the amount of radioactivity released into the culture supernatants by the cells. The radioactivity in the culture supernatants increased rapidly (Fig. 8*Ba*), and the increase was quantitatively correlated with a decrease in the cell-bound radioactivity (Fig. 8*Bb*). The radioactivity in the culture supernatants of BAFβ-mHP2 clones was similar to that of BAFβ clones (Fig. 8*Ba*), but the amounts of the degraded short pep-

tides obtained by TCA precipitation in the culture supernatants of BAFβ-mHP2 cells were apparently lower than those in the culture supernatants of BAFβ cells (Fig. 8*Bc*). We also tried to examine the kinetics of ^{125}I-IL-4 degradation in the BAF-B03 transfectants. However, we found that a small amount of ^{125}I-IL-4 was dissociated from the receptors during the indicated incubation times. Therefore, we used a chemical cross-linker to link ^{125}I-IL-4 and the receptor. In degradation analyses, the radioactivity in the culture supernatants of BAF-IL-4Rα-mH cells was lower than that in the culture supernatants of BAF-IL-4Rα cells (Fig. 8*C*, *a* and *b*). Furthermore, the amounts of the degraded short peptides in the culture supernatants of BAF-IL-4Rα-mH cells were apparently lower than those in the culture supernatants of BAF-IL-4Rα cells (Fig. 8*Cc*). The degradation patterns of the antibodies against the receptors in the transfectants were similar to those of the ligands, suggesting that the antibodies were delivered by the same endosomal sorting route as the ligands. Therefore, these findings support the possibility that the hydrophobic amino acid clusters of the receptors are required for their accurate transport to the lysosome for degradation.

On the other hand, the kinetics on the tyrosine phosphorylations of STAT5 and STAT6, downstream molecules of IL-2R and IL-4R, respectively, were similar between the wild-type and mutant receptor expressing cells (supplemental Fig. S4, *A* and *B*). The kinetics on the tyrosine phosphorylations of IL-2Rβ and IL-4Rα were also similar between the wild-type and mutant receptor expressing cells (supplemental Fig. S4, *A* and *B*). The difference of the receptor degradation pattern between the wild-type and mutant IL-2Rβ (or IL-4Rα) became marked after 120 min (Fig. 7), whereas the tyrosine phosphorylations of the
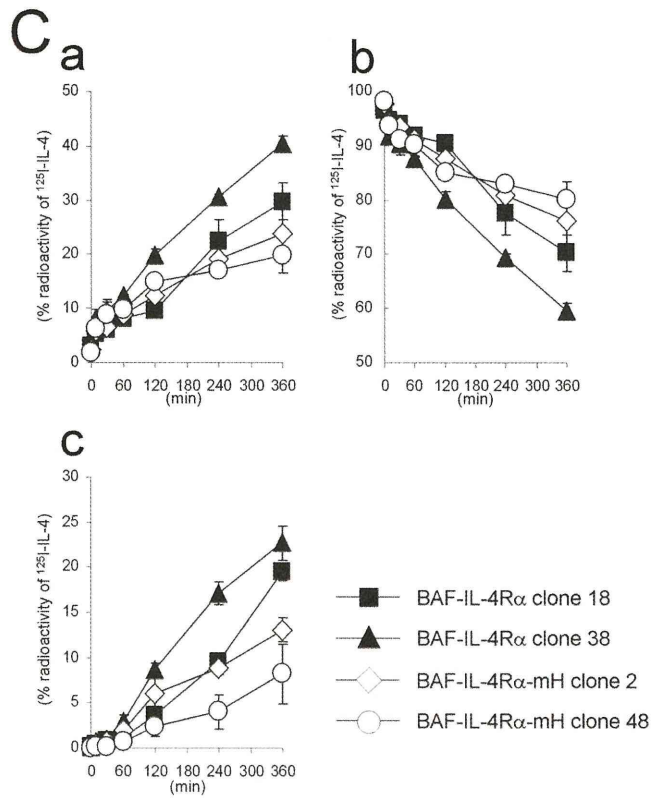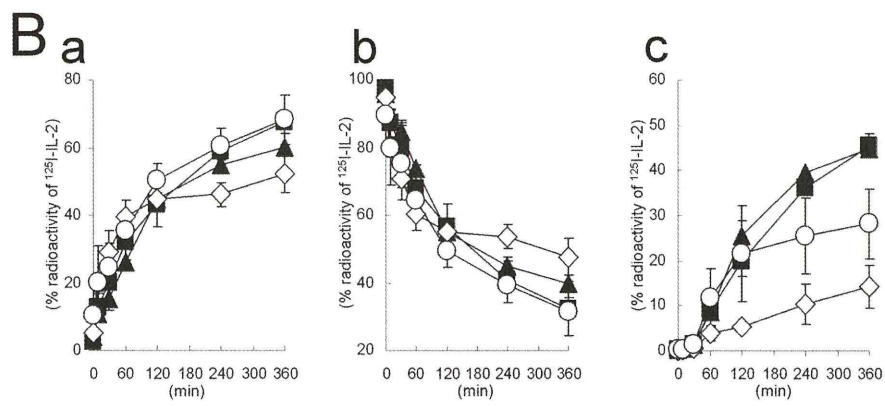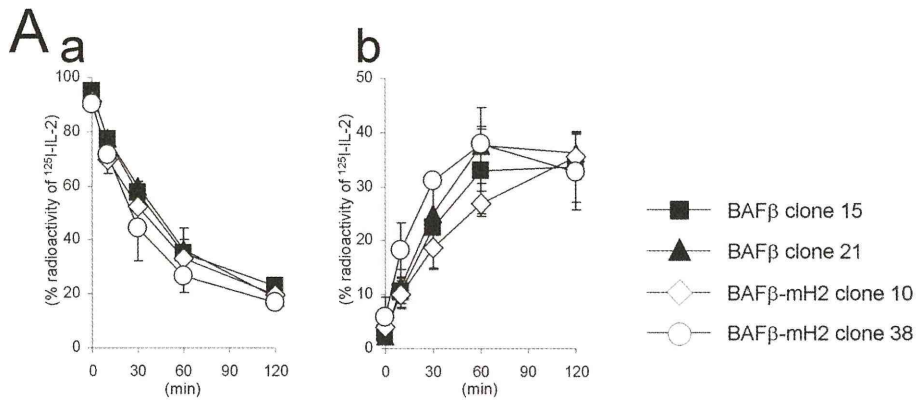
receptors and the STAT molecules by the ligand stimulations were observed within 120 min. Thus, the kinetics on the tyrosine phosphorylations of these molecules may not be influenced by the differences between the wild-type and mutant receptor degradations.

Because functional IL-2R and IL-4R are composed of a combination of each the receptor subunit and IL-2Rγc, we examined whether IL-2Rγc is colocalized with each the subunit using a confocal microscope. Similar to the case of wild-type IL-2Rβ in MEFβ cells, IL-2RβmH2 expressed in MEFβ-mH2 was colocalized with IL-2Rγc under steady-state conditions in the presence of IL-2 (supplemental Fig. S5A). The degree of the colocalization between IL-2Rγc and IL-4RαmH in MEF-IL-4Rα-mH cells was also similar to that of the colocalization between IL-2Rγc and wild-type IL-4Rα in MEF-IL-4Rα cells in the presence of IL-4 (supplemental Fig. S5B). At 40 min after the ligand stimulation, wild-type IL-2Rβ had been departed from transferrin receptor-positive early endosomes as described previously (23). We then tried to examine the colocalization between IL-2Rβ and IL-2Rγc departed from early endosomes and here found that wild and the mutant IL-2Rβ were colocalized with IL-2Rγc at 40 min after IL-2 stimulation (supplemental Fig. S5C). These observations suggested that IL-2Rγc and its receptor counterpart stably exist in the same compartments during the course of the endosomal sorting.

The Mutant Receptors Lacking the Hydrophobic Amino Acid Cluster Are Localized to LBPA-positive Compartments Rather than LAMP1-positive Compartments—The data shown in Fig. 5, C and D, indicated that although the wild-type receptors were localized to LAMP1-positive compartments, the receptors lacking the hydrophobic amino acid cluster were found as punctuate structures that differed from the LAMP1-positive compartments. Previously, we reported that an IL-2Rβ mutant lacking amino acids 349–410, which includes the hydrophobic amino acid cluster, is partially mis-sorted to transferrin receptor-positive recycling endosomes, resulting in interference with its transport to LAMP1-positive compartments (23). Similar to the result of IL-2Rβ mutant lacking amino acids 349–410, the receptors lacking the hydrophobic amino acid cluster were also partially mis-sorted to transferrin receptor-positive recycling endosomes in the kinetics study of these receptors (supplemental Fig. S6). However, the localization of the mutant at recycling endosomes was hardly detectable under steady-state conditions. Thus, we further searched for the subcellular localizations of IL-2RβmH2 and IL-4RαmH under steady-state conditions. LBPA is a component of luminal vesicles in late endosomes and a marker of MVBs (34, 35). Therefore, using the MEF transfectant MEFβ-mH2, MEFβ, MEF-IL-4Rα-mH, and MEF-IL-4Rα cells, we tried to compare the ratios of mutant receptors localized to LAMP1-positive compartments with
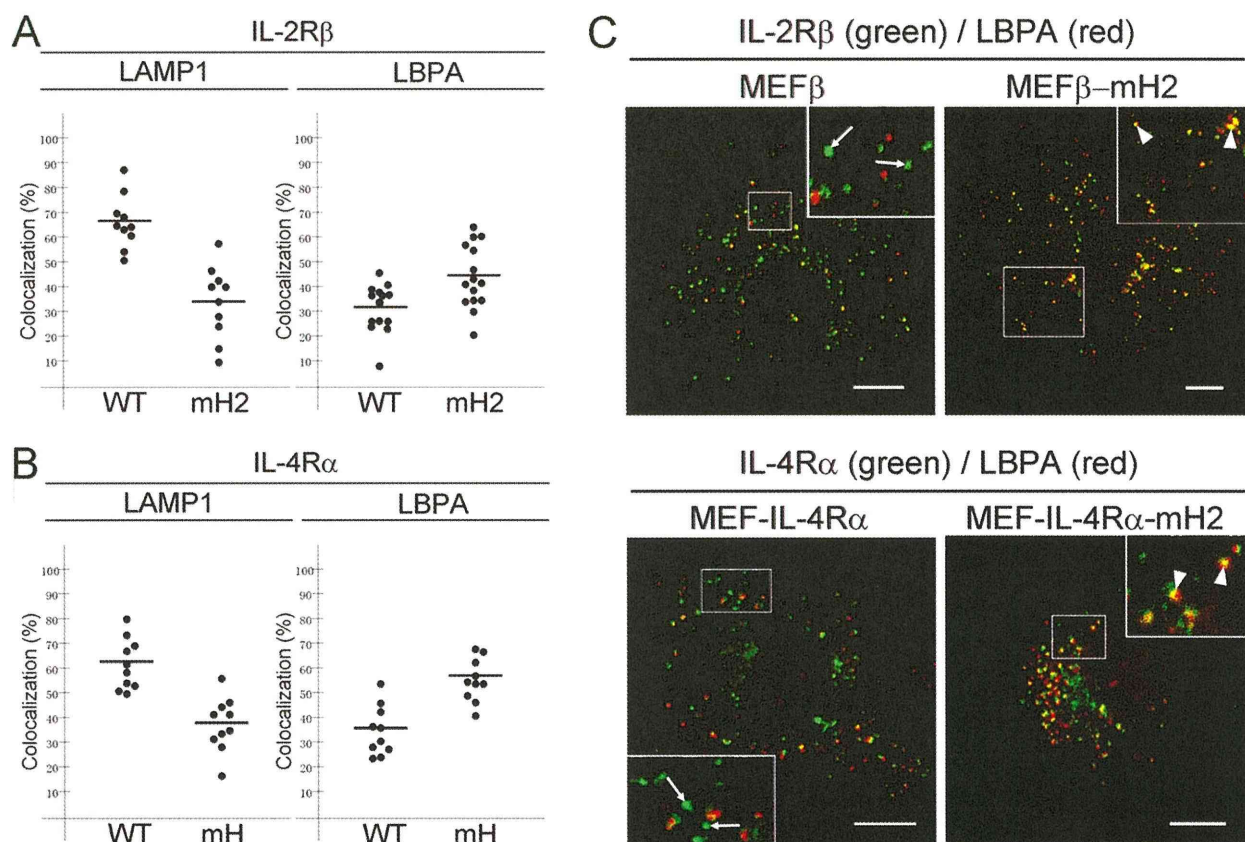
those localized to LBPA-positive compartments. Consistent with the results shown in Fig. 5, wild-type IL-2Rβ expressed in MEFβ cells was colocalized with 66% of LAMP1-positive compartments, whereas IL-2RβmH2 lacking the hydrophobic amino acid cluster expressed in MEFβ-mH2 cells was colocalized with 34% of LAMP1-positive compartments (Fig. 9A). In contrast, wild-type IL-2Rβ was colocalized with 32% of LBPA-positive compartments, whereas IL-2RβmH2 was colocalized with 44% of LBPA-positive compartments (Fig. 9, A and C). Similar results were obtained for the localizations of IL-4Rα in MEF-IL-4Rα cells and IL-4RαmH in MEF-IL-4Rα-mH cells. Wild-type IL-4Rα and IL-4RαmH lacking the hydrophobic amino acid cluster were colocalized with 62 and 38% of LAMP1-positive compartments, respectively (Fig. 9B), whereas wild-type IL-4Rα and IL-4RαmH were colocalized with 35 and 56% of LBPA-positive compartments, respectively (Fig. 9, B and C). These findings suggest that some of the mutant receptors lacking the hydrophobic amino acid cluster are localized to LBPA-positive compartments rather than LAMP1-positive compartments and that the transport of the mutant receptors to LAMP1-positive compartments is partially impaired, resulting in accumulation of the mutant receptors in LBPA-positive compartments.

DISCUSSION

The Hydrophobic Amino Acid Cluster Is a Ubiquitin-independent Endosomal Sorting Signal—The present results indicate that the hydrophobic amino acid cluster is an Hrs binding motif on the basis of our analyses of two cytokine receptors and functions as an endosomal sorting signal for the receptors. There are currently two major endosomal sorting signal sequences, namely Y$XX\phi$ and (D/E)XXXL(L/I), which are the consensus motifs for tyrosine-based and dileucine-based signals, respectively (1). Both sequences are recognized by the adaptor protein (AP) complexes AP-1, AP-2, AP-3, and AP-4. Y$XX\phi$ signal sequences are widely found in molecules not only at the plasma membrane (36, 37) but also at the trans-Golgi network (38) and lysosome (39, 40), suggesting multiple roles in endosomal sorting. Y$XX\phi$ signal sequences, one of which is located in the cytoplasmic region of transferrin receptor (41), play an essential role for the internalization of membrane proteins. Another type of tyrosine-based signal sequence (NPXY) is often found in membrane molecules such as low density lipoprotein receptor, insulin receptor, and epidermal growth factor receptor and is involved in the internalization but not other endosomal sorting events of a subset of type I integral membrane proteins (42). (D/E)XXXL(L/I) signal sequences are found in type I, type II, and multispanning transmembrane proteins, which are widely distributed from the plasma membrane to late endosomes, lysosomes, and specialized antigen-process-

---

FIGURE 8. **Internalization and degradation of ^{125}I-IL-2 and ^{125}I-IL-4 in BAF-B03 transfectants.** *A,* internalization of ^{125}I-IL-2 in the transfectants is shown. BAF transfectants were incubated with 350 pM ^{125}I-IL-2 at 0 °C. The cells were then cultured at 37 °C and harvested at the indicated times. The radioactivities of the cell surface-bound acid-removable fractions (*a*) and intracellular acid-unremovable fractions (*b*) were counted. *B,* degradation of ^{125}I-IL-2 in the transfectants is shown. BAF transfectants were incubated with 350 pM ^{125}I-IL-2 and then cultured for the indicated times. The radioactivities of the culture supernatants (*a*), cell precipitate fractions (*b*), and TCA-soluble fractions of the culture supernatants (*c*) were counted. *C,* degradation of ^{125}I-IL-4 in the transfectants is shown. BAF transfectants were incubated with 250 pM ^{125}I-IL-4, treated with the cross-linker DTSSP, and then cultured for the indicated times. The radioactivities of the culture supernatants (*a*), cell precipitate fractions (*b*), and TCA-soluble fractions of the culture supernatants (*c*) were counted. The values represent the means ± S.E. of three separate experiments.

FIGURE 9. **Localizations of IL-2Rβ and IL-4Rα mutants lacking the hydrophobic amino acid cluster to LBPA-positive compartments.** MEF transfectants were grown on coverslips, fixed, and double-labeled with an anti-IL-2Rβ antibody (C20) or anti-IL-4Rα antibody (C20) and an anti-LAMP1 monoclonal antibody or anti-LBPA monoclonal antibody. Fluorescence images of the MEF transfectants ($n \geq 10$ cells) were captured using a confocal laser microscope. The percentages of the IL-2Rβ-positive (*A*) and IL-4Rα-positive (*B*) pixel areas that were colocalized with LAMP1 (*left*) and LBPA (*right*) were analyzed. *C*, the IL-2Rβ-positive and IL-4Rα-positive pixel areas that were colocalized with LBPA (*arrowheads*) and not with LBPA (*arrows*) are indicated. Fluorescence labeling was carried out for IL-2Rβ (*green*), IL-4Rα (*green*), and LBPA (*red*). *Scale bars,* 10 μm.

ing compartments, similar to YXXϕ signal sequences. For example, the (D/E)XXXL(L/I) signal sequence in the CD3-γ chain mediates its rapid internalization and lysosomal targeting (43), and internalization of glucose transporter 8 is mediated by the interaction of (D/E)XXXL(L/I) signal sequence with AP2 complex (44), indicating that (D/E)XXXL(L/I) signal sequence plays a essential role for the internalization in the membrane proteins. In contrast, the hydrophobic amino acid clusters found in this study were involved in the interaction with Hrs and not needed for the internalization of the receptors. Another type of dileucine-based signal sequence (DXXLL) is present in molecules at the plasma membrane, trans-Golgi network, and endosomes and is recognized by another family of adaptor proteins known as Golgi-localized γ-ear-containing Arf-binding proteins (GGAs). The DXXLL sequence interacts with the VHS domain of GGAs (45, 46). On the other hand, the VHS domains of both Hrs and STAM bind to ubiquitin but not the DXXLL sequence (45, 47). Regarding other signal sequences, acidic amino acid clusters are present in some transmembrane proteins and are considered to play roles in their retrieval from endosomes to the trans-Golgi network (1). The hydrophobic amino acid cluster identified in this study is unique in the following points; (i) the cluster is involved in ubiquitin-independent sorting (ii) the cluster is recognized by Hrs, a known sort-

ing component of the ubiquitin-dependent machinery ESCRT-0, and (iii) the cluster comprises FFFHL in IL-2Rβ and LFLDLL in IL-4Rα, indicating that the amino acid sequence of the cluster may vary a great deal. Thus, we speculate that Hrs may recognize the hydrophobic amino acid clusters in various receptors with broad specificity. In this regard, our analyses to identify a key domain (amino acids 428–466) in Hrs that influences the receptor binding are important. Although there is no motif involved in the protein-protein interaction, we focused on a hydrophobic amino acid cluster comprising amino acids 453–457 (LLELL) in the C-terminal half of Hrs. We generated an Hrs mutant with the hydrophobic amino acids (residues 453–457) with alanine and examined the binding between this Hrs mutant and IL-2Rβ or IL-4Rα. Only slight reductions in the associations of the Hrs mutant with the receptors were observed (data not shown). Accordingly, extensive analyses, including solution of the crystallographic structure, will be needed to explore this region (amino acids 428–466) of Hrs. Recently, the complete crystal structure of human ESCRT-0 core complex was clarified (48). Analyses of the crystal structure revealed that the coiled-coil domains of Hrs and STAM form an antiparallel two-stranded coiled-coil. The coiled-coil domain of Hrs consists of four α-helix strands, α1 (amino acids 406–429), α2 (amino acids 432–436), α3-N (amino acids 437–

453), and α3-C (amino acids 470 – 498). Because the hydrophobic amino acid cluster binding region (residues 428 – 466) of Hrs includes the hinge region between α1 and α2, the area around the hinge region may be a candidate site that contributes to the interaction.

On the other hand, what are the biological features of the receptors that are recognized by Hrs in a ubiquitin-independent manner? The epidermal growth factor receptor is localized on the cell surface membrane in the absence of ligand stimulation, and receptor internalization and transport to the MVB pathway are initiated following receptor ubiquitylation after ligand stimulation (49 – 52). In contrast, IL-2Rβ is constitutively internalized and delivered to the lysosomal pathway in the absence of its ligand (23). We found that IL-4Rα as well as IL-2Rβ was localized to LAMP1-positive compartments without ligand stimulation, suggesting constitutive internalization and endosomal sorting of IL-4Rα. Consequently, we speculate that the ubiquitin-independent binding targets of Hrs may be certain kinds of receptors that have the properties of constitutive internalization and sorting to lysosomes.

In conclusion, ESCRT complexes including ESCRT-0, which consists of Hrs and STAM, serve as the transport machinery for ubiquitylated cargo proteins. Therefore, it is noteworthy that Hrs associates with cytokine receptors in a ubiquitin-independent manner and is involved in their transport during endosomal sorting. In the present study we found that Hrs recognized a hydrophobic amino acid cluster in two cytokine receptors and played a role in the precise delivery of the receptors to late endosomes. These findings suggest the existence of a group of cargo proteins that are independent of ubiquitylation for endosomal sorting and have the hydrophobic amino acid cluster as an endosomal sorting signal motif.

REFERENCES

1. Bonifacino, J. S., and Traub, L. M. (2003) *Annu. Rev. Biochem.* **72,** 395– 447
2. Di Fiore, P. P., Polo, S., and Hofmann, K. (2003) *Nat. Rev. Mol. Cell. Biol.* **4,** 491– 497
3. Hicke, L., Schubert, H. L., and Hill, C. P. (2005) *Nat. Rev. Mol. Cell. Biol.* **6,** 610 – 621
4. Katzmann, D. J., Babst, M., and Emr, S. D. (2001) *Cell* **106,** 145–155
5. Alam, S. L., Sun, J., Payne, M., Welch, B. D., Blake, B. K., Davis, D. R., Meyer, H. H., Emr, S. D., and Sundquist, W. I. (2004) *EMBO J.* **23,** 1411–1421
6. Slagsvold, T., Aasland, R., Hirano, S., Bache, K. G., Raiborg, C., Trambaiolo, D., Wakatsuki, S., and Stenmark, H. (2005) *J. Biol. Chem.* **280,** 19600 – 19606
7. Hanson, P. I., Roth, R., Lin, Y., and Heuser, J. E. (2008) *J. Cell Biol.* **180,** 389 – 402
8. Lata, S., Schoehn, G., Jain, A., Pires, R., Piehler, J., Gottlinger, H. G., and Weissenhorn, W. (2008) *Science* **321,** 1354–1357
9. Teis, D., Saksena, S., and Emr, S. D. (2008) *Dev. Cell* **15,** 578 – 589
10. Saksena, S., Wahlman, J., Teis, D., Johnson, A. E., and Emr, S. D. (2009) *Cell* **136,** 97–109
11. Wollert, T., Wunder, C., Lippincott-Schwartz, J., and Hurley, J. H. (2009) *Nature* **458,** 172–177
12. Komada, M., and Kitamura, N. (1995) *Mol. Cell. Biol.* **15,** 6213 – 6221
13. Takeshita, T., Arita, T., Asao, H., Tanaka, N., Higuchi, M., Kuroda, H., Kaneko, K., Munakata, H., Endo, Y., Fujita, T., and Sugamura, K. (1996) *Biochem. Biophys. Res. Commun.* **225,** 1035–1039
14. Asao, H., Sasaki, Y., Arita, T., Tanaka, N., Endo, K., Kasai, H., Takeshita, T., Endo, Y., Fujita, T., and Sugamura, K. (1997) *J. Biol. Chem.* **272,** 32785–32791
15. Lloyd, T. E., Atkinson, R., Wu, M. N., Zhou, Y., Pennetta, G., and Bellen, H. J. (2002) *Cell* **108,** 261–269
16. Polo, S., Sigismund, S., Faretta, M., Guidi, M., Capua, M. R., Bossi, G., Chen, H., De Camilli, P., and Di Fiore, P. P. (2002) *Nature* **416,** 451– 455
17. Raiborg, C., Bache, K. G., Gillooly, D. J., Madshus, I. H., Stang, E., and Stenmark, H. (2002) *Nat. Cell Biol.* **4,** 394 – 398
18. Mizuno, E., Kawahata, K., Kato, M., Kitamura, N., and Komada, M. (2003) *Mol. Biol. Cell* **14,** 3675 – 3689
19. Raiborg, C., and Stenmark, H. (2009) *Nature* **458,** 445– 452
20. Bishop, N., Horman, A., and Woodman, P. (2002) *J. Cell Biol.* **157,** 91–101
21. Shih, S. C., Katzmann, D. J., Schnell, J. D., Sutanto, M., Emr, S. D., and Hicke, L. (2002) *Nat. Cell Biol.* **4,** 389 – 393
22. Sugamura, K., Asao, H., Kondo, M., Tanaka, N., Ishii, N., Ohbo, K., Nakamura, M., and Takeshita, T. (1996) *Annu. Rev. Immunol.* **14,** 179 – 205
23. Yamashita, Y., Kojima, K., Tsukahara, T., Agawa, H., Yamada, K., Amano, Y., Kurotori, N., Tanaka, N., Sugamura, K., and Takeshita, T. (2008) *J. Cell Sci.* **121,** 1727–1738
24. Takeshita, T., Asao, H., Ohtani, K., Ishii, N., Kumaki, S., Tanaka, N., Munakata, H., Nakamura, M., and Sugamura, K. (1992) *Science* **257,** 379 – 382
25. Suzuki, J., Takeshita, T., Ohbo, K., Asao, H., Tada, K., and Sugamura, K. (1989) *Int. Immunol.* **1,** 373 – 377
26. Tanaka, Y., Tozawa, H., Hayami, M., Sugamura, K., and Hinuma, Y. (1985) *Microbiol. Immunol.* **29,** 959 – 972
27. Ishii, N., Takeshita, T., Kimura, Y., Tada, K., Kondo, M., Nakamura, M., and Sugamura, K. (1994) *Int. Immunol.* **6,** 1273 – 1277
28. Fraker, P. J., and Speck, J. C., Jr. (1978) *Biochem. Biophys. Res. Commun.* **80,** 849 – 857
29. Gillooly, D. J., Raiborg, C., and Stenmark, H. (2003) *Histochem. Cell Biol.* **120,** 445 – 453
30. Radhakrishna, H., and Donaldson, J. G. (1997) *J. Cell Biol.* **139,** 49 – 61
31. Taniguchi, T., and Minami, Y. (1993) *Cell* **73,** 5 – 8
32. Harada, N., Yang, G., Miyajima, A., and Howard, M. (1992) *J. Biol. Chem.* **267,** 22752 – 22758
33. Ohbo, K., Takeshita, T., Asao, H., Kurahayashi, Y., Tada, K., Mori, H., Hatakeyama, M., Taniguchi, T., and Sugamura, K. (1991) *J. Immunol. Methods* **142,** 61 – 72
34. Kobayashi, T., Stang, E., Fang, K. S., de Moerloose, P., Parton, R. G., and Gruenberg, J. (1998) *Nature* **392,** 193 – 197
35. Matsuo, H., Chevallier, J., Mayran, N., Le Blanc, I., Ferguson, C., Fauré, J., Blanc, N. S., Matile, S., Dubochet, J., Sadoul, R., Parton, R. G., Vilbois, F., and Gruenberg, J. (2004) *Science* **303,** 531 – 534
36. Canfield, W. M., Johnson, K. F., Ye, R. D., Gregory, W., and Kornfeld, S. (1991) *J. Biol. Chem.* **266,** 5682 – 5688
37. Jadot, M., Canfield, W. M., Gregory, W., and Kornfeld, S. (1992) *J. Biol. Chem.* **267,** 11069 – 11077
38. Humphrey, J. S., Peters, P. J., Yuan, L. C., and Bonifacino, J. S. (1993) *J. Cell Biol.* **120,** 1123 – 1135
39. Williams, M. A., and Fukuda, M. (1990) *J. Cell Biol.* **111,** 955 – 966
40. Harter, C., and Mellman, I. (1992) *J. Cell Biol.* **117,** 311 – 325
41. Marks, M. S., Woodruff, L., Ohno, H., and Bonifacino, J. S. (1996) *J. Cell Biol.* **135,** 341 – 354
42. Chen, W. J., Goldstein, J. L., and Brown, M. S. (1990) *J. Biol. Chem.* **265,** 3116 – 3123
43. Letourneur, F., and Klausner, R. D. (1992) *Cell* **69,** 1143 – 1157
44. Schmidt, U., Briese, S., Leicht, K., Schürmann, A., Joost, H. G., and Al-Hasani, H. (2006) *J. Cell Sci.* **119,** 2321 – 2331